HHS Public Access

Author manuscript

Nature. Author manuscript; available in PMC 2024 June 12.

Published in final edited form as:

Nature. 2023 August ; 620(7972): 154–162. doi:10.1038/s41586-023-06358-0.

Neural basis for fasting activation of hypothalamic-pituitary-adrenal axis

Amelia M. Douglass[1,**], **Jon M. Resch**[1,5,**], **Joseph C. Madara**[1,**], **Hakan Kucukdereli**[1], **Ofer Yizhar**[3], **Abhinav Grama**[4], **Masahito Yamagata**[4], **Zongfang Yang**[1], **Bradford B. Lowell**[1,2,*]

[1]Division of Endocrinology, Diabetes and Metabolism, Department of Medicine, Beth Israel Deaconess Medical Center, Harvard Medical School, Boston, MA, USA

[2]Program in Neuroscience, Harvard Medical School, Boston, MA, USA

[3]Departments of Brain Sciences and Molecular Neuroscience, Weizmann Institute of Science, Rehovot, Israel

[4]Center for Brain Science, Department of Molecular and Cellular Biology, Harvard University, Cambridge, MA, USA

[5]Current Address: Department of Neuroscience and Pharmacology, University of Iowa Carver College of Medicine, Iowa City, IA, USA

Summary

Fasting initiates a multitude of adaptations to allow survival. Activation of the hypothalamic-pituitary-adrenal (HPA) axis and subsequent release of glucocorticoid hormones is a key response that mobilizes fuel stores to meet energy demands[1-5]. Despite the importance of the HPA axis response, the neural mechanisms that drive its activation during energy deficit are unknown. Here, we show that fasting-activated hypothalamic agouti-related peptide (AgRP)-expressing neurons trigger and are essential for fasting-induced HPA axis activation. AgRP neurons do so via projections to the paraventricular hypothalamus (PVH), where, in a mechanism not previously described for AgRP neurons, they presynaptically inhibit the terminals of tonically active GABAergic afferents from the bed nucleus of the stria terminalis (BNST) that otherwise restrain activity of corticotrophin-releasing hormone (CRH)-expressing neurons. This disinhibition of PVH^{Crh} neurons requires GABA (γ-aminobutyric acid)/GABA-B receptor signaling and potently activates the HPA axis. Importantly, stimulation of the HPA axis by AgRP neurons is independent of their induction of hunger, showing that these canonical 'hunger neurons' drive multiple adaptations to the fasted state. Together our findings identify the neural basis for fasting-induced HPA axis activation and uncover a unique means by which AgRP neurons activate

[*]**Materials and Correspondence** to Bradford B. Lowell. (blowell@bidmc.harvard.edu).

[**]Co-first author

Author contributions

A.M.D., J.M.R. and B.B.L. conceived the study and designed experiments. J.C.M. performed and analyzed slice electrophysiology experiments. A.M.D. and H.K. performed and analyzed fiber photometry experiments. O.Y. provided the AAV-eOPN3 and guidance on its use. A.G. and M.Y. made the AAV-synaptophysin-GCaMP6f. A.M.D. and J.M.R. performed and analyzed all other experiments and prepared the figures. Z.Y. assisted with stereotaxic surgeries. A.M.D., J.M.R. and B.B.L. wrote the manuscript with input from all authors.

Competing interests

The authors declare no competing interests.

downstream neurons – via presynaptic inhibition of GABAergic afferents. Given the potency of this disinhibition of tonically-active BNST afferents, other activators of the HPA axis, such as psychological stress, may also work by reducing BNST inhibitory tone onto PVH^{Crh} neurons.

Introduction

Fasting triggers behavioral, physiologic and metabolic responses which collectively are vital for survival. One of these is activation of the HPA axis (Extended Data Fig. 1a)[1-5] which increases blood levels of adrenal glucocorticoid (GC) hormones – cortisol in humans[5] and corticosterone in rodents[1-4]. This adaptive response serves to prevent fasting-induced drops in blood glucose[3,4,6]. Absence of this response during fasting, in humans with reduced adrenal function[6,7] or when GC function is blocked in rodents[3] impairs key metabolic responses, leading to hypoglycemia. Glucocorticoid hormones maintain glucose homeostasis by a series of interconnected, combined effects; by directly stimulating glucose-synthesizing gluconeogenic pathways in the liver[8,9], by mobilizing gluconeogenic precursors from muscle protein[10], and by stimulating lipolysis in adipocytes[3,11]- the latter of which generates glycerol, yet another gluconeogenic precursor, and free fatty acids that are then used as alternative fuel by peripheral tissues, sparing the limited glucose supply for the brain.

Despite the importance of fasting-activation of the HPA axis, the mechanism that causes this is unknown. That said, it appears to be triggered by a fall in the adipose tissue-derived hormone leptin[1-3]. Given that AgRP-expressing neurons within the arcuate nucleus of the hypothalamus (ARC) are activated by fasting, in part by leptin deficiency, and that numerous other adaptive responses triggered by fasting are also caused by increased AgRP neuron activity[12-14], we hypothesized that AgRP neurons are responsible for fasting-activation of the HPA axis. A recent publication attempted to address this hypothesis but obtained conflicting results[15] and therefore, whether AgRP neurons regulate the HPA axis is unknown, as is the mechanism by which they might bring about such regulation.

Results

AgRP neurons activate the HPA axis

The HPA axis is strongly activated by fasting and is inversely related to levels of leptin[1,3]. We confirmed that plasma corticosterone, which is strongly elevated in 24-hour fasted mice, is suppressed by leptin (Extended Data Fig. 1b-d). Since AgRP neuron activity is increased by fasting and low leptin, we asked whether it is indeed the increased AgRP neuron activity that is actually responsible for increasing plasma corticosterone. To activate AgRP neurons, we expressed hM3Dq bilaterally in the ARC of *Agrp*-IRES-Cre mice (Fig. 1a, Extended Data Fig. 3a, b). Trunk blood was collected 1 hour after clozapine-*N*-oxide (CNO) injection during the early light cycle when endogenous corticosterone is low (Fig. 1b). Activation of AgRP neurons in *ad libitum* fed animals substantially increased plasma corticosterone (Fig. 1c). Conversely, inhibition of AgRP neurons using hM4Di completely suppressed fasting-levels of corticosterone (Fig. 1a, d, e, Extended Data Fig. 3c, d). Together these data demonstrate that leptin-sensitive AgRP neurons drive corticosterone release and are vitally important for this response during fasting.

Release of GCs occurs by step-wise activation of the HPA axis, with the first step in the pathway being excitation of PVH^{Crh} neurons[16] (Extended Data Fig. 1a). To assess whether AgRP neurons activate the HPA axis we recorded intracellular calcium levels from PVH^{Crh} neurons as a proxy for neuronal activity, via fiber photometry, while simultaneously activating AgRP neurons using CNO/hM3Dq (Fig. 1f, g, Extended Data Fig. 3e). The I.P. injection itself caused a brief stress response but, only CNO injection in mice expressing hM3Dq in AgRP neurons drove rapid and sustained activation of PVH^{Crh} neurons (Fig. 1h, i), which was not observed in mice expressing mCherry in AgRP neurons (Fig. 1j, k). Importantly, inhibition of AgRP neurons in fasted animals reduced PVH^{Crh} neuron activity (Fig. 1f, l, m). This effect is likely partial given incomplete transduction of AgRP neurons with hM4Di (Extended Data Fig. 3f, g) due to the small volumes of AAV necessary to avoid DREADD expression in PVH^{Crh} neurons in *Agrp*-IRES-Cre::*Crh*-IRES-Cre mice. Finally, consistent with engagement of the HPA axis, brief optogenetic stimulation of AgRP neurons strongly increased plasma adrenocorticotropic hormone (ACTH) as well as corticosterone (Fig. 1n, q; Extended Data Fig. 1e, f, Extended Data Fig. 3h, i). Thus, AgRP neurons drive corticosterone release via the HPA axis.

HPA axis activation is independent of hunger

Given that PVH^{Crh} neurons are the apex of the HPA axis, we hypothesized that PVH-projecting AgRP neurons cause activation of the HPA axis. To test this, we optogenetically stimulated discrete projection fields of AgRP neurons *in vivo* using bilateral expression of Channelrhodopsin-2 (ChR2) (Fig. 2a, b, Extended Data Fig. 4a-d, Extended Data Fig. 5a-d). Stimulation of AgRP terminals in the PVH, and also surprisingly in the BNST and lateral hypothalamus (LH), all caused similar increases in plasma corticosterone (Fig. 2c). In contrast, stimulation of terminals in the parabrachial nucleus (PBN) had no effect (Fig. 2c). Coincidentally, the same AgRP neuron projections that activate the HPA axis, i.e., to the BNST, LH and PVH, also have been shown to cause hunger[17]. This raises the possibility that it is stimulation of hunger itself, a motivational drive state that is aversive[18], that actually causes HPA axis activation. To address this possibility, we looked one synapse downstream in the pathway by which AgRP neurons cause hunger – at the PVH melanocortin 4 receptor (MC4R)-expressing satiety neurons. These neurons, when inhibited by AgRP neurons, cause hunger[19]. Importantly, direct bilateral CNO/hM4Di-mediated inhibition of PVH^{Mc4r} neurons increased food intake (Extended Data Fig. 1g, h, Extended Data Fig. 10b, c) but did not affect plasma corticosterone (Extended Data Fig. 1i, j). Thus, hunger itself does not activate the HPA axis. Instead, HPA axis activation must be a distinct action of AgRP neurons that is independent of their ability to inhibit downstream PVH (MC4R-expressing) satiety neurons.

The PVH is the site of AgRP neuron action

AgRP neurons are proposed to be largely wired in a one-to-one manner, with different subsets of AgRP neurons projecting to different downstream sites[17]. If this is the case, then our ChR2 terminal stimulation of AgRP neurons (Fig. 2c) suggests that there exists in each of these downstream sites, the PVH, BNST and LH, neurons that when inhibited by AgRP neuron projections, activate the HPA axis. At first glance, this might be unexpected as the apex of the HPA axis, CRH neurons, lie in just one of these downstream sites, the PVH.

If, on the other hand, there is a sufficient degree of collateralization in projections to the BNST, LH and PVH, then it is possible that optogenetic stimulation of axons in either the BNST or the LH antidromically activate collaterals that project to the PVH. Given the importance of this issue with regards to interpreting our ChR2 terminal stimulation studies, we used two approaches to assess collateralization of AgRP neuron projections. In the first, we injected a retrograde AAV-FlpO into distinct projection fields of AgRP neurons in Cre- and Flp-dependent GFP reporter mice (*Agrp*-IRES-Cre::FLTG) (Fig. 2d). The resulting GFP expression marks the projections, including all collaterals of AgRP neurons that project to the site of AAV-FlpO injection. This revealed that BNST- and LH-projecting AgRP neurons do indeed send some collaterals to the PVH (Fig. 2e, Extended Data Fig. 2a, b). PBN-projecting AgRP neurons, on the other hand, collateralize only in the periaqueductal gray (PAG) (Extended Data Fig. 2a, b). Recall that stimulation of AgRP terminals in the PBN failed to activate the HPA axis. Our second approach for looking at collaterals, rabies-based collateral mapping, yielded similar results (Extended Data Fig. 2c, d). Hence, in agreement with the prior study[17], AgRP neurons are largely wired in a one-to-one fashion but there is some degree of collateralization in AgRP neurons that project to the LH, BNST and PVH. Given the existence of these collaterals, our ChR2 terminal stimulation studies are unable to establish whether neurons in the PVH, LH and/or BNST mediate AgRP neuron activation of the HPA axis. To examine this issue in a way not confounded by the existence of collaterals, we used a terminal-based inhibition approach. Specifically, we selectively inhibited synaptic transmission by AgRP neuron terminals using a light-activated $G_{i/o}$-coupled inhibitory opsin, eOPN3[20], and looked at effects on fasting activation of the HPA axis (Fig. 2f, g, Extended Data Fig. 6a-f). Importantly, bilateral terminal specific inhibition of AgRP projections in the PVH, but not in the LH or BNST, significantly reduced fasting levels of corticosterone (Fig. 2h). These data strongly suggest that AgRP neurons activate the HPA axis via their projections to the PVH.

AgRP neurons disinhibit PVH^{Crh} neurons

We next investigated how AgRP neurons drive activity of PVH^{Crh} neurons. This is a particularly compelling question because AgRP neurons release only inhibitory neurotransmitters (GABA, neuropeptide Y (NPY) and AgRP) and therefore are unlikely to activate the HPA axis via direct excitation of PVH^{Crh} neurons. Consistent with this, as assessed using ChR2-assisted circuit mapping, AgRP neurons do not make monosynaptic connections with PVH^{Crh} neurons, while they do make monosynaptic connections with PVH^{Mc4r} neurons which they inhibit to produce hunger[19]. Alternatively, AgRP neurons could activate PVH^{Crh} neurons by inhibiting an intermediate, tonically active GABAergic afferent. Given that the PVH is the key site of AgRP neuron regulation of the HPA axis (Fig. 2h) and that all PVH neurons are glutamatergic[21], we hypothesized that AgRP neurons inhibit GABAergic tone onto PVH^{Crh} neurons by inhibiting the terminals of such GABAergic afferents. Of interest, prior studies have shown that NPY can reduce inhibitory tone onto unidentified PVH neurons[22,23] and in other parts of the brain[24]. Similarly, GABA acting on presynaptic GABA-B-Rs reduces electrically-evoked GABA release onto PVH^{Crh} neurons[25]. To re-examine this, we recorded electrically-evoked inhibitory post-synaptic currents (eIPSCs) onto PVH^{Crh} neurons *ex vivo* using *Crh*-IRES-Cre::tdTomato mice to identify the CRH neurons (Fig. 3a). eIPSCs were assessed before and after bath application

of NPY or the GABA-B receptor (GABA-B-R) agonist baclofen. We excluded a role for PVH melanocortin receptors, and hence released AgRP, because hM3Dq-mediated activation of ARC proopiomelanocortin (POMC) neurons, which release the MC3/4R agonist α-MSH, did not reduce corticosterone in the fasted state (Extended Data Fig. 1k-m, Extended Data Fig. 10d, e). This indicates that AgRP signaling at PVH melanocortin receptors is unlikely to be involved in driving the HPA axis. Consistent with the prior studies, bath application of NPY or baclofen, markedly reduced the amplitude of eIPSCs (Fig. 3b-d, g, h). Both effects were entirely blocked by application of an NPY2R or GABA-B-R antagonist (Fig. 3e, f, i). Further, NPY and baclofen both increased paired-pulse ratio while input resistance was unchanged, further demonstrating that both modulate presynaptic release (Fig. 3j-m). Thus, NPY and GABA can mediate presynaptic inhibition via their receptors located on GABAergic afferents to PVH^{Crh} neurons. We then probed the relative importance of GABA-B-Rs and NPY2Rs by testing whether baclofen and NPY have additive effects on eIPSC amplitude. Baclofen application further suppressed eIPSC amplitude after NPY treatment, while NPY did not have an additive effect when applied after baclofen (Fig. 3n-p). These data suggest that GABA-B-Rs are likely expressed more densely and/or on a greater number of PVH^{Crh} neuron afferent terminals compared to NPY2Rs, and that GABA-B-Rs may play a more prominent role in the disinhibition of PVH^{Crh} neurons by AgRP neurons.

Next, we tested if NPY and GABA are required for AgRP neurons to activate the HPA axis. We optogenetically stimulated AgRP neurons in the absence of NPY (*Agrp*-IRES-Cre::NPY-KO mice) or in mice in which the vesicular GABA transporter, *Slc32a1* (vGAT), was selectively removed from AgRP neurons (*Agrp*-IRES-Cre::vGAT$^{lox/lox}$ mice) to prevent AgRP neuron-mediated GABA release (Fig. 4a, b, Extended Data Fig. 7a-d). The corticosterone response upon AgRP neuron stimulation was still intact in the absence NPY or vGAT but was entirely lost in the double knockout animals (Fig. 4c). Intriguingly, the corticosterone response to stimulation of AgRP neurons was blunted in *Agrp*-IRES-Cre::vGAT$^{lox/lox}$ mice compared to *Agrp*-IRES-Cre::NPY-KO mice. This, along with our *ex vivo* pharmacology data (Fig. 3n-p), demonstrates that GABA release from AgRP neurons acting on GABA-B-Rs may play a greater role in activation of the HPA axis than NPY. To explore this idea further, we next asked whether NPY and/or GABA signaling in the PVH specifically is required for the fasting increase in HPA axis activity. We infused NPY2R (BIIE0246) and/or GABA-B-R (Saclofen) antagonists into the PVH of fasted mice (Fig. 4d, e, Extended Data Fig. 8a-d). Although vehicle infusion itself caused high corticosterone levels in fed mice presumably due to the stress of infusion, blockade of NPY2Rs had no effect on the further elevation of corticosterone caused by fasting, while the GABA-B-R antagonist alone and in combination with the NPY2R antagonist strongly reduced fasting levels of plasma corticosterone (Fig. 4f). All together these data support a model where GABA release from AgRP neurons acting on GABA-B-R-expressing afferents in the PVH is required to activate the HPA axis. However, given that NPY can compensate to some degree when GABA is chronically absent in *Agrp*-IRES-Cre::vGAT$^{lox/lox}$ animals[26] and is sufficient to activate the HPA axis when injected into the PVH[27], we cannot eliminate a role for NPY/NPY2Rs. Furthermore, the potential redundancy between GABA and NPY demonstrates the importance of preserving this vital adaptation to the fasted state.

BNST (GABA) axon terminals are inhibited

We next sought to identify the source of GABAergic input to PVH^{Crh} neurons that is inhibited by AgRP neurons. It is widely understood that the HPA axis is controlled by GABAergic afferent neurons that are tonically active and thus constrain the excitability of PVH^{Crh} neurons[28-31]. We therefore identified the putative sites of GABAergic input specifically to PVH^{Crh} neurons by performing EnvA pseudotyped monosynaptic rabies mapping (Extended Data Fig. 2e). Our rabies mapping revealed many putative afferents to PVH^{Crh} neurons and several of these rabies-labelled brain regions are known to contain GABAergic neurons (Extended Data Fig. 2f-j.). Of these areas, the BNST is regarded as a key modulator of HPA axis activity, with the anteroventral BNST in particular having been shown to act as an inhibitory brake on the HPA axis[32,33]. ChR2-assisted circuit mapping verified that BNST^{vGAT} neurons potently inhibit PVH neurons, directly inhibiting both PVH^{Crh} neurons and PVH$^{non\text{-}Crh}$ neurons (Fig. 5a, b). Therefore, we hypothesized that AgRP neurons excite PVH^{Crh} neurons by inhibiting BNST axon terminals in the PVH. If so, inhibition of BNST^{vGAT} neurons should stimulate the HPA axis. Indeed, chemogenetic inhibition of BNST^{vGAT} neurons in vGAT-IRES-Cre mice strongly increased plasma corticosterone to levels seen in fasted animals (Fig. 5c-e, Extended Data Fig. 9a, b). Similar inhibition of LH GABAergic neurons, however, was without effect (Fig. 5c-e, Extended Data Fig. 9c, d). We next performed terminal-specific inhibition of BNST^{vGAT}PVH projections using eOpn3 (Fig. 5f-h, Extended Data Fig. 9e). eOpn3 prevents presynaptic neurotransmission via the $G_{i/o}$ pathway in the same manner as GABA and NPY acting on GABA-B-Rs[20] and NPY2Rs[34], respectively, thus perfectly mimicking the effect of these transmitters released from AgRP neurons on BNST^{vGAT}PVH neuron terminals. Terminal inhibition of BNST^{vGAT}PVH neurons robustly stimulated plasma corticosterone (Fig. 5i). Thus, inhibition of BNST^{vGAT} PVH terminals disinhibits PVH^{Crh} neurons and strongly activates the HPA axis.

Finally, we asked if AgRP neurons do indeed inhibit BNST axon terminals in the PVH. We performed fiber photometry recordings from BNST neuron terminals in the PVH using a GCaMP targeted to synaptic terminals (synaptophysin-targeted GCaMP6f) while optogenetically stimulating AgRP neuron terminals through the same fiber using ChrimsonR (Fig. 5j, k, Extended Data Fig. 10a). Stimulation of AgRP neurons with red light, rapidly and dramatically suppressed BNSTPVH synaptic GCaMP signal which recovered after cessation of the stimulation (Fig. 5l-n). Furthermore, AgRP neuron terminal varicosities are abundant and clearly in close proximity to BNST axon terminals and PVH^{Crh} neuron somas within the PVH (Fig. 5o). Thus, AgRP neurons presynaptically inhibit BNST neuron terminals in the PVH. Together these data support a model where tonically active inhibitory afferents from the BNST strongly suppress PVH^{Crh} neuron activity under non-fasting conditions. During fasting, elevated AgRP neuron activity and subsequent release of GABA into the PVH causes presynaptic inhibition of these BNST afferents. Ultimately, this reduces GABAergic tone onto PVH^{Crh} neurons, potently stimulating the HPA axis (Fig. 5p).

Discussion

Activation of the HPA axis is an essential adaptive response to energy deficit. In response to a fast, the ensuing increase in blood glucocorticoids is important to maintain glucose homeostasis and supply metabolic substrates for use as fuel sources. Though clearance of glucocorticoids may be slowed during fasting[35], the basis for fasting activation of the HPA axis had been unknown. Here, we provide a neural mechanism for fasting-induced glucocorticoid release by establishing that AgRP neurons drive the HPA axis. Through a mechanism novel for AgRP neurons, they do so by releasing GABA into the PVH to engage GABA-B-Rs on GABAergic afferents to PVH^{Crh} neurons, reducing GABAergic input onto PVH^{Crh} neurons. Furthermore, we identified the presynaptic terminals of BNST^{vGAT} neurons as a specific target of AgRP neurons, which causes disinhibition of PVH^{Crh} neurons, driving their activity and a surge in corticosterone. Importantly, we also show that AgRP neuron control of the HPA axis occurs in parallel to and via a downstream neural pathway distinct from AgRP neuron-driven hunger and feeding. Together these data reveal important mechanisms underlying AgRP neuron function in driving critical adaptive responses to energy deficit.

Disinhibition drives the HPA axis

The activity of PVH^{Crh} neurons and the HPA axis is thought to be constrained by tonically active GABAergic afferents[28-31]. It therefore follows that activation of the HPA axis requires removal of tonic inhibition to allow excitation of PVH^{Crh} neurons. Here, we provide strong evidence that disinhibition of GABAergic afferents to PVH^{Crh} neurons potently causes HPA axis activation. PVH^{Crh} neurons are excited by AgRP neuron-mediated release of GABA and NPY, which activate GABA-B-Rs and NPYRs on presynaptic terminals of GABAergic BNST neurons in the PVH. This presynaptic inhibition of GABA release, or disinhibition, reduces GABAergic tone onto PVH^{Crh} neurons and causes their activation. A role for such presynaptic disinhibition is supported by a number of observations. First, NPY and GABA reduce inhibitory tone onto PVH^{Crh} neurons in *ex vivo* brain slices (Fig. 3 and [22,23,25]). Second, *in vivo* eOpn3 inhibition of BNST terminals in the PVH potently increases glucocorticoids. Of note, eOpn3 inhibits presynaptic transmission by blocking calcium channel activity[20] through a $G_{i/o}$ pathway, thus, closely mimicking the effects of GABA/GABA-B-Rs and NPY/NPYRs on BNST terminals. And third, activation of AgRP neurons potently inhibits BNSTPVH neuron terminals. Together, these data show that GABA and NPY released from AgRP neurons act on GABA-B-Rs and NPYRs on BNSTPVH neuron terminals to reduce their activity, thus preventing release of GABA and relieving inhibition of PVH^{Crh} neurons.

Although we have established that GABA and NPY are individually sufficient to reduce GABAergic transmission onto PVH^{Crh} neurons *ex vivo*, *in vivo* we found infusion of a GABA-B-R antagonist into the PVH was alone sufficient to profoundly reduce corticosterone levels during fasting. Furthermore, AgRP neuron-mediated corticosterone release was reduced in mice lacking vGAT (hence GABA release) compared to mice that lack NPY, which is consistent with more potent suppression of GABAergic tone onto PVH^{Crh} neurons by GABA/GABA-B-Rs. Together these data support a more prominent

role for GABA in AgRP neuron-driven activation of the HPA axis. Nevertheless, AgRP neuron-mediated corticosterone release was totally abolished only in the absence of both vGAT and NPY in *AgRP*-IRES-Cre::vGAT$^{lox/lox}$::NPY-KO mice. It is noteworthy that using an identical gene knockout approach, AgRP neuron stimulation of hunger was found to similarly depend on both NPY and GABA[26]. In our study, the presence of a corticosterone response after AgRP neuron stimulation in single knockout animals, although reduced in mice lacking vGAT, suggests redundancy between GABA and NPY, or that knockout of either transmitter during development can be functionally compensated for at least in part by the other. Given that NPY has prolonged effects on feeding[36], it is also possible that NPY released by AgRP neurons primarily serves to sustain HPA activity levels during prolonged fasting[37]. Of note, NPY infusion into the PVH is sufficient to drive HPA activity and PVH-projecting hindbrain catecholaminergic neurons containing NPY are required to activate the HPA axis in response to hypoglycemia[27,38]. Therefore, NPY engagement of NPYR-expressing terminals of GABAergic afferents to PVH^{Crh} neurons may play a more prominent role under these conditions. Nevertheless, given the importance of HPA axis activation in the fasted state, the potential for redundancy between GABA and NPY highlights that preserving release of glucocorticoids during fasting is crucial.

In this study, we discovered that disinhibition of PVH^{Crh} neurons underlies HPA axis activation during fasting. However, it is plausible that relief of BNST-derived GABAergic tone onto PVH^{Crh} neurons is a common means via which the HPA axis is activated by other stressors. In support of this, we found that terminals of BNST neurons in the PVH are also inhibited by a startling stimulus (Extended Data Fig. 2k, l). This indicates that the BNST may be a crucial circuit node through which a variety of stressful conditions drive glucocorticoid release. How this pathway might be recruited in response to acute stressors or more chronic states such as anxiety is an area for future investigation. In addition, our monosynaptic rabies mapping revealed that a number of brain areas contain putative PVH^{Crh} neuron afferents, several of which are known to contain GABA neurons. It is conceivable that additional sources of GABA may also inhibit the HPA axis and that these may also be inhibited by AgRP neurons during fasting. The precise identity of these afferents to PVH^{Crh} neurons and their role in HPA axis activation during fasting and other conditions will be an important area for further study

Dual actions of AgRP neurons in the PVH

AgRP neurons activate the HPA axis through their projections to the PVH where they cause excitation of PVH^{Crh} neurons. This is particularly striking because AgRP neurons only release inhibitory neurotransmitters (GABA, NPY and AgRP) and previous reports have demonstrated that AgRP neurons regulate their downstream targets via direct inhibition[14,19,39,40]. Notably, the PVH is also the site where AgRP neurons cause hunger via monosynaptic inhibition of PVH^{Mc4r} and PVH^{Pdyn} neurons[19,41]. Thus, AgRP neurons can inhibit or excite different neurons in the same downstream area by direct inhibition or by modulating neurotransmission onto neurons with which they do not form synapses (Fig. 5p). Inhibition of PVH^{Mc4r} and PVH^{Pdyn} neurons to drive hunger is caused by direct synaptic contacts and engagement of GABA-A-Rs and NPYRs on the postsynaptic neurons. Consistent with PVH^{Crh} neurons mediating fasting and AgRP neuron activation of the HPA

axis, but not hunger[19], they are not directly inhibited by AgRP neurons and are instead activated via the presynaptic disinhibition mechanism described above. In the absence of synaptic contact, levels of GABA are likely too low to engage GABA-A-Rs on PVH^{Crh} neurons which have much lower affinity for GABA than GABA-B-Rs[42,43]. In addition, PVH^{Crh} neurons express low levels of NPYRs (unpublished data and, ref. [44], Extended Data Fig. 2m). As a result, GABA-B-R-mediated inhibition of GABAergic afferents to PVH^{Crh} neurons is the principal mechanism of AgRP neuron action on PVH^{Crh} neurons. A previous study reported that 52% of AgRP neuron boutons in the PVH do not form post-synaptic contacts[45]– perhaps this is the source of GABA reaching GABA-B-Rs on BNST GABAergic inputs to PVH^{Crh} neurons. Our data demonstrates that AgRP neurons have both direct and indirect modes of synaptic regulation within one downstream brain region. It is therefore possible that extra-synaptic release of transmitter from AgRP neurons at other sites in the brain may also contribute to differing effects on the activity of neurons in these areas and importantly, on the activity of their inputs. Together our findings in the PVH, and the differential control of hunger versus HPA axis activation, have wide-reaching implications for our understanding of how AgRP neurons coordinate specific activation and inhibition of functionally diverse neurons within the same downstream site.

Glucocorticoids activate AgRP neurons

In light of the importance of AgRP neurons in driving the HPA axis and corticosterone release, it is notable that AgRP neurons themselves are also activated *by* corticosterone and that this causes hunger and food intake[46]. Thus, AgRP neuron activity is driven by and also stimulates corticosterone release. We speculate that this could be a key aspect of their regulation and that sustained activity of AgRP neurons during fasting may in part be mediated by corticosterone and maintained by this positive feedback loop.

In summary, our work has revealed that activation of AgRP neurons causes HPA axis induction during fasting. In doing so, we have expanded our understanding of AgRP neuron function during fasting, and we have shed light on how AgRP neurons can both directly inhibit and indirectly activate key downstream target neurons. Moreover, we have also established an important mechanism of HPA axis activation, by providing concrete evidence that presynaptic inhibition of tonically active inhibitory afferent tone from the BNST is a critical physiologic driver of HPA axis activation (Fig. 5p).

Methods

Animals

All animal care and experimental procedures were approved by the Institutional Animal Care and Use Committees at Beth Israel Deaconess Medical Center and the University of Iowa. Prior to experiments mice were housed at 22-24°C, 20-30% humidity with a 12:12 light:dark cycle Mice had *ad libitum* access to chow (Envigo Teklad F6 8664) and water unless otherwise stated. Mice were singly housed at least one week prior to the start of experiments.

Male mice (8-20 weeks) were used for hormone measurement and fiber photometry experiments except for *AgRP*-IRES-Cre::vGAT$^{lox/lox}$::NPY-KO experiments where both male and female mice were used due to low likelihood of obtaining mice of the correct genotype. Both male and female mice were also used for anatomical and electrophysiological studies. C57BL6/J (JAX stock 000664), *Agrp*-IRES-Cre[47] (JAX stock 012899), *Crh*-IRES-Cre[48], *Mc4r*-t2a-Cre[19] (JAX stock 030759), *Pomc*-IRES-Cre[49], vGAT-IRES-Cre[50] (JAX stock 016962), *Crh*-IRES-FlpO (JAX stock 031559), *R26-loxSTOPlox-L10*-GFP[48], Ai32(RCL-ChR2(H134R)/EYFP)[51] (JAX stock 024109), Ai9(lox)-tdTomato[51] (JAX stock 007909), RC:FLTG[52] (JAX stock 026932), vGAT$^{lox/lox}$[47] (JAX stock 012897), NPY-KO[53] (JAX stock 004545) mice were maintained on a mixed background.

AAV construction

AAV2/9-hSyn-synaptophysin-GCaMP6f-WPRE was prepared and obtained from the University of Pennsylvania Vector Core. The rat synaptophysin-GCaMP6f was constructed from rat synaptophysin[54] and GCaMP6f[55] sequences by Gibson assembly (NEBuilder HiFi DNA Assembly, NEB) and enzymatically cloned into an AAV backbone with a human synapsin I promoter[56]. The pAAV-hSyn-synaptophysin-GCaMP6f- WPRE plasmid is available from Addgene (Plasmid #102996).

Stereotaxic surgeries

Mice were anesthetized with xylazine (10 mg per kg) and ketamine (100 mg per kg) diluted in 0.9% sterile isotonic saline and placed into a stereotaxic apparatus (KOPF model 940). For postoperative care, mice were injected subcutaneously with sustained-release meloxicam (4 mg per kg). After exposing the skull via small incision, a small hole was drilled for injection. A pulled-glass pipette with 20–40 μm tip diameter was inserted into the brain and virus was injected by an air pressure system controlled by a Grass Technologies stimulator (model S48) to deliver injections at 25 nl min^{-1}. The pipette was withdrawn 5 min after injection.

For the arcuate, AAV was injected at 6 sites to cover the anterior-posterior extent of the arcuate (50 nl per site, bregma: AP: −1.5 mm and −1.7 mm, DV: −5.90 mm, ML: −0.25 mm, 0 mm, +0.25 mm). For photometry experiments, AAV was injected into the arcuate at 4 sites to prevent excessive spread (50 nl per site, bregma: AP: −1.5 mm and −1.7 mm, DV: −5.90 mm, ML: −0.25 mm and + 0.25 mm). For the PVH, 20 nl per site was injected at bregma, AP: −0.9 mm, DV: −4.8 mm, ML: ±0.16 mm. For the BNST, 20nl per site was injected at bregma, AP: +0.55 mm, DV: −4.8 mm, ML: ±0.65 mm. For the LH, 20nl per site was injected at bregma, AP: −1.5 mm, DV: −5.0 mm, ML: ±1.2 mm.

Animals were allowed to recover from stereotaxic surgery a minimum of 21 days prior to experiments. Following each experimental procedure, accuracy of AAV injections was confirmed via post hoc histological analysis of XFP reporters. All subjects determined to be surgical “misses” based on little or absent reporter expression were removed from analyses.

For chemogenetic experiments, AAV8-hSyn-DIO-mCherry (University of North Carolina (UNC) Vector Core; 2.1 × 10^{13} viral genomes ml^{-1}), AAV8-hSyn-DIO-hM3Dq-mCherry (Boston Children’s Hospital (BCH) Viral Core) or AAV8-hSyn-DIO-hM4Di-mCherry (BCH

Viral Core; 2×10^{13} viral genomes ml^{-1}) were injected bilaterally into the arcuate of *Agrp*-IRES-Cre or *Pomc*-IRES-Cre mice; the PVH of *Mc4r*-2a-Cre mice; the BNST or LH of vGAT-IRES-Cre mice.

To label PVH^{Crh} neuron somas, AAV1-Ef1a-Cre(ON)/Flp(OFF) 2.0-BFP (Addgene 137130-AAV1; 2.24×10^{13} viral genomes ml^{-1}) was injected into the PVH of *Crh*-IRES-Cre mice.

For optogenetics experiments, AAV8-hSyn-DIO-mCherry (UNC Vector Core; 2.1×10^{13} viral genomes ml^{-1}), AAV9-EF1a-DIO-ChR2(H134R)-mCherry (Addgene 20297-AAV9; 2.5×10^{13} viral genomes ml^{-1}), AAV1-hSyn2-SIO-eOPN3-mScarlet-WPRE (Addgene 125713-AAV1; 1×10^{13} viral genomes ml^{-1}) or AAV5-Syn-FLEX-rc[ChrimsonR-tdTomato] (Addgene 62723-AAV5; 2.1×10^{13} viral genomes ml^{-1}) was injected bilaterally into the arcuate of *Agrp*-IRES-Cre mice, *Agrp*-IRES-Cre::NPY-KO mice, *Agrp*-IRES-Cre::vGAT$^{lox/lox}$ or *AgRP*-IRES-Cre::vGAT$^{lox/lox}$::NPY-KO mice or the BNST of vGat-IRES-Cre mice. AAV9-EF1a-DIO-ChR2(H134R)-eYFP (Addgene 26973-AAV9; 2.2×10^{13} viral genomes ml^{-1}) was injected into the BNST of vGAT-IRES-Cre::*Crh*-IRES-FlpO::FLTG mice.

For fiber photometry experiments, AAV1-hSyn-DIO-GCaMP6s (Addgene 100845- AAV1; 1.6×10^{13} viral genomes ml^{-1}) was injected bilaterally into the PVH of *Agrp*-IRES-Cre::*Crh*-IRES-Cre mice. AAV2/9-hSyn-synaptophysin-GCaMP6f-WPRE (3.62×10^{13} viral genomes ml^{-1}) was injected into the BNST of *Agrp*-IRES-Cre mice.

Optic fiber implants—For optogenetic experiments targeting the cell bodies of AgRP neurons, an optic fiber (200 μm diameter core; R-FOC_L200C-39NA; NA 0.39; RWD Life Science) was implanted at the midline over AgRP neurons (AP: −1.6 mm, DV: −5.85 mm, ML: 0 mm) of *Agrp*-IRES-Cre::LSL-ChR2-eYFP and *Agrp*-IRES-Cre::lox-L10-GFP mice or *Agrp*-IRES-Cre::NPY-KO, *Agrp*-IRES-Cre::vGAT$^{lox/lox}$ or *AgRP*-IRES-Cre::vGAT$^{lox/lox}$::NPY-KO mice injected with AAV9-EF1a-DIO-ChR2(H134R)-mCherry. For AgRP neuron terminal stimulation experiments, optic fibers fiber (200 μm diameter core; R-FOC_L200C-39NA; NA 0.39; RWD Life Science) were implanted over one of the AgRP neuron terminal fields: PVH (AP: −0.9 mm, DV: −4.6 mm, ML: 0 mm), BNST (AP: +0.55 mm, DV: −4.35 mm, ML: −0.65 mm), LH (AP: −1.5 mm, DV: −4.5 mm, ML: −1.2 mm) or bilaterally over the PBN (AP: −5.25 mm, DV: −3.0 mm, ML: ±1.5 mm) of *Agrp*-IRES-Cre mice injected with AAV8-hSyn-DIO-mCherry or AAV9-EF1a-DIO-ChR2(H134R)-mCherry.

For AgRP neuron terminal inhibition experiments, optic fibers (200 μm diameter core; R-FOC_L200C-39NA; NA 0.39; RWD Life Science) were implanted over one of the AgRP neuron terminal fields: PVH (AP: −0.9 mm, DV: −4.6 mm, ML: 0 mm), BNST (AP: +0.55 mm, DV: Left −3.83 mm (angled at 20°) and Right −4.35 mm, ML: Left −2.19 mm (angled at 20°) and Right +0.65 mm), LH (AP: −1.5 mm, DV: −4.5 mm, ML: ±1.2 mm) of *Agrp*-IRES-Cre mice injected with AAV8-hSyn-DIO-mCherry or AAV1-hSyn2-SIO-eOPN3-mScarlet-WPRE.

For BNST terminal inhibition experiments, a single optic fiber (200 μm diameter core; R-FOC_L200C-39NA; NA 0.39; RWD Life Science) was implanted over the PVH (AP: −0.9 mm, DV: −4.6 mm, ML: 0 mm) of vGAT-IRES-Cre mice injected with AAV1-hSyn2-SIO-eOPN3-mScarlet-WPRE or AAV8-hSyn-DIO-mCherry.

For fiber photometry recordings, an optic fiber (400 um diameter core; MFC_400/430-0.66_7mm_MF1.25_FLT; NA 0.66; Doric Lenses) was placed over the PVH (AP: −0.9, DV: −4.7, ML: −0.15).

Fibers were fixed to the skull using dental acrylic. Following experiments and histology of the brain tissue, the location of the fiber tips were identified.

Monosynaptic rabies mapping—For monosynaptic rabies mapping, AAV8-Ef1a-FLEX-TVA-mCherry (UNC Vector Core; 1.13 x 10^{12} viral genomes ml^{-1}) and AAV8-CAG-FLEX-rabiesG (Stanford Vector Core; 3.4 x 10^{12} viral genomes ml^{-1}) (mixed 1:1, 20 nl) were injected into the PVH of *Crh*-IRES-Cre using the coordinates above. After three weeks, the mice underwent a second surgery where 20 nl EnvA-ΔG-rabies-GFP (Salk Viral Vector Core; 1.51 x 10^{8} viral genomes ml^{-1}) was injected into the PVH. 6 days following rabies virus injection the mice were processed for histological analysis.

Collateral mapping—For TVA-only rabies mapping, AAV8-Ef1a-FLEX-TVA-mCherry was injected into the arcuate of *Agrp*-IRES-Cre mice using the coordinates above. After three weeks, EnvA-ΔG-rabies-GFP (10-100 nl per site) was injected into one of the following AgRP neuron terminal fields: PVH (AP: −0.9 mm, DV: −4.8 mm, ML: ±0.16 mm), BNST (AP: +0.55 mm, DV: −4.8 mm, ML: ±0.65 mm), LH (AP: −1.5 mm, DV: −5.0 mm, ML: ±1.2 mm), PBN (AP: −5.3 mm, DV: −3.5 mm, ML: ±1.7 mm). Animals were perfused 6 days after injection of the rabies virus.

For retro-AAV-based collateral mapping, retroAAV-EF1a-FlpO (Addgene 55637-AAVrg; 1.02 x 10^{13} viral genomes ml^{-1}) (10-100nl per site) was injected into AgRP neuron terminal fields (as for TVA-only rabies mapping) of *Agrp*-IRES-Cre::FLTG mice. Animals were perfused 4 weeks post injection. Presence of collaterals was performed by immunofluorescent detection of GFP and analysis of all AgRP neuron projection fields.

Infusion cannula implants and *in vivo* pharmacology

Bilateral intrahypothalamic guide cannula (C235G, 26G, 3.25 mm length, P1 Technologies) were implanted at the midline above the PVH of C57Bl6/J mice (AP: −0.9, ML: ±0.25, DV: −3.25). Cannula were fixed to the skull using dental acrylic. Bilateral dummy cannula (C235DC, 26G, 3.25 mm + 0.5 mm projection, P1 Technologies) were placed into the guide cannula until experiments.

Microinjection of antagonists into the PVH was performed in freely-moving mice. Mice were habituated to tethering for two days prior to experiments. Bilateral internal cannula (C2351, 33G, 3.25 mm + 1.5 mm projection, P1 Technologies) were placed into the guide cannula and connected to infusion tubing (C232CT, P1 Technologies) via a connector (C230C/SPC, P1 Technologies). Infusion tubing was connected to a Hamilton syringe (22G,

1 μl) controlled by a syringe pump (NE-4000 New Era). Prior to experiments, the mice were placed into a fresh home cage and fasted for 24 hours, from 1 hour prior to the onset of the dark cycle. GABA-B-R antagonist (2-hydroxysaclofen, 3.1 mM per side, Tocris), NPY2R antagonist (BIIE0246, 0.5 mM per side, Tocris), GABA-B-R + NPY2R antagonists or vehicle (10% DMSO, Sigma) were infused over 2 hours at a rate of 10 nl per minute per side (total volume 1.2 μl). Immediately after infusions the mice were rapidly decapitated for trunk blood collection and brains were collected for histological assessment of guide cannula location.

Optogenetic experiments

All optogenetic experiments were performed with singly housed animals in the presence of food unless otherwise stated.

For optogenetic stimulation of AgRP neurons and terminals with ChR2, mice were tethered to optic fiber patch cords in the home cage and allowed to acclimate for 2 hours prior to experiments. The mice received photostimulation (473 nm; 10 ms pulses of 20 Hz at ~10mW; 1 s ON, 3 s OFF) for 10 minutes, after which they were rapidly decapitated and trunk blood was collected. Experiments were performed 4 hours after the onset of the light phase.

For optogenetic inhibition of AgRP neuron terminals with eOPN3, mice were placed into a fresh home cage and fasted for 24 hours from 1 hour prior to the onset of the dark cycle. The next day, 3 hours prior to the dark phase, the mice were tethered to optic fiber patch cords and received photoinhibition (473 nm, 10 ms pulses at 10Hz at ~5mW, 2 s ON, 2 s OFF) for 2 hours, after which they were rapidly decapitated and trunk blood was collected.

To optogenetically inhibit $BNST^{vGAT}$ neuron terminals in the PVH with eOPN3, mice were tethered to optic fiber patch cables 1 hour after the onset of the light cycle. After 1 hour the stimulation commenced (473 nm, 10 ms pulses at 10Hz ~5mW, 2 s ON, 2 s OFF) for 1 hour, after which the mice were rapidly decapitated and trunk blood was collected.

Chemogenetic experiments

For measurements in the fed state, *Agrp*-IRES-Cre mice expressing hM3Dq or mCherry in the arcuate, vGAT-IRES-Cre mice expressing hM4Di or mCherry in the BNST or LH were injected I.P. with CNO (1 mg kg^{-1}; 0.5% body weight volume) two hours after the onset of the light cycle. One hour later the mice were rapidly decapitated and trunk blood was collected. Experiments were performed in the presence of food.

For PVH^{Mc4r} neuron inhibition, *Mc4r*-t2a-Cre mice expressing hM4Di or mCherry in the PVH were first tested for increased food intake by injecting vehicle or CNO (1 mg kg^{-1}; 0.5% body weight volume) I.P. two hours after the onset of the light cycle and measuring food intake over the following three hours. One week later, the same mice were injected with CNO two hours after the onset of the light cycle and were rapidly decapitated for trunk blood collection one hour later. Experiments were performed in the presence of food.

For measurements in the fasted state, *Agrp*-IRES-Cre mice expressing hM4Di or mCherry in the arcuate and *Pomc*-IRES-Cre mice expressing hM3Dq and mCherry in the arcuate were placed into a fresh home cage and fasted for 24 hours, from one hour prior to the onset of the dark cycle. One hour prior to sacrifice, mice were injected I.P. with CNO. The mice were then rapidly decapitated and trunk blood was collected.

Leptin treatment—C57BL6 mice were placed into a fresh home cage and fasted for 24 hours, from 1 hour prior to the onset of the dark cycle. 1.5 hours prior to sacrifice, mice were injected I.P. with vehicle or recombinant leptin (5 mg/kg). The mice were rapidly decapitated and trunk blood was collected.

Hormone Measurements—Collected trunk blood was centrifuged for plasma collection. Plasma was run in duplicate in a 96 well plate enzyme-linked immunosorbent assay (ELISA) kit for corticosterone (Enzo Life Sciences) according to the manufacturer's protocol. ACTH was measured using radioimmunoassay by the Brigham Research Assay Core (Brigham and Woman's Hospital).

Fiber photometry

Fiber photometry was performed using a Micropython microcontroller-based pyPhotometry[57] acquisition system. 465 nm and 405 nm LED (Doric Lenses) excitation sources were passed through a fluorescence mini cube (Excitation: 460-490 nm and 400-410 nm, Emission: 500-550nm, Doric Lenses). The excitation light was transmitted onto the sample via an optic fiber cable (1 m long; 400 μm diameter NA 0.48; Doric Lenses) coupled to the implanted optic fiber via a ceramic mating sleeve (Thor Labs). Light intensity at the end of the patch cord (30-60 μW) was kept constant across sessions for each mouse. Time-division multiplexed illumination was performed at 20Hz and the signal was collected by a photodetector (Doric lenses) and digitized by the Micropython acquisition board.

Recordings were performed in *Agrp*-IRES-Cre::*Crh*-IRES-Cre mice that express AAV1-hSyn-DIO-GCaMP6s in the PVH and AAV8-hSyn-DIO-hM3Dq-mCherry, AAV8-hSyn-DIO-hM4Di-mCherry or AAV8-hSyn-DIO-mCherry in the arcuate. Experiments were performed within-subject with each animal receiving 2 x vehicle and 2 x CNO (1 mg/kg) trial in counterbalanced order with at least 3 days between trials for experiments in which AgRP neurons were activated. For experiments where AgRP neurons were inhibited, fasted mice received 1 x vehicle and 1 x CNO injection with 5 days recovery between trials. Mice were habituated to tethering and I.P. injection for two days prior to the first recording.

Recordings from BNST terminals in the PVH were performed concurrent with AgRP neuron stimulation through the same optic fiber. 465 nm, 405 nm LED (Doric Lenses) and 630 nm (Plexon) excitation sources were passed through a fluorescence mini cube (Photometry Excitation: 460-490 nm and 400-410 nm, Optogenetic Excitation: 580-680 nm, Photometry Emission: 500-540nm, Doric Lenses). For fiber photometry recordings, time-division multiplexed illumination was performed at 20 Hz. Optogenetic stimulation was interleaved between the 465 and 405 nm pulses at 20 Hz to prevent cross-talk between the stimulation and fiber photometry recording using an Arduino board running custom

code synchronized to the pyPhotometry system. Signal was collected by a photodetector (Newport 2151) and digitized by the Micropython acquisition board.

Fiber photometry analysis—Fiber photometry data was analyzed using a custom Python (Python 3.6) script. All data were median filtered and low pass filtered (10Hz cutoff). Photobleaching was corrected by fitting an exponential curve to the data and subtracting it from the signal. Motion correction was performed by finding a linear best fit to the 405 nm signal and subtracting this from the 465 nm signal. ΔF/F was calculated as (465 nm – 405 nm fitted signal) / F0, where F0 is the low-pass filtered 465 nm signal (0.001 Hz cutoff) of the whole recording session. For experiments where CNO/Saline was administered IP, trials were renormalized by subtracting the mean of the 5 minute baseline prior to the injection from the trace following IP injection. All trials of a treatment type were averaged to calculate the mean response (0-5 minutes pre-injection and 0-30 minutes after IP injection). Signals from recordings performed with optogenetic stimulation experiments were renormalized by subtracting the mean either a 50 second or 5 minute baseline prior to onset of the 630 nm stimulus. Traces were finally smoothed using a 10 second running average.

Electrophysiology

To prepare *ex vivo* murine brain slices, animals were deeply anesthetized with isoflurane before decapitation and removal of the entire brain. Brains were immediately submerged in ice-cold, carbogen-saturated (95% O_2, 5% CO_2) choline-based cutting solution consisting of (in mM): 92 choline chloride, 10 HEPES, 2.5 KCl, 1.25 NaH_2PO_4, 30 $NaHCO_3$, 25 glucose, 10 $MgSO_4$, 0.5 $CaCl_2$, 2 thiourea, 5 sodium ascorbate, 3 sodium pyruvate, oxygenated with 95% O_2/5% CO_2, measured osmolarity 310 – 320 mOsm/L, pH= 7.4. Then, 275-300 μm-thick coronal sections were cut with a vibratome (Campden 7000smz-2) and incubated in oxygenated cutting solution at 34°C for 10 min. Next, slices were transferred to oxygenated aCSF (126 mM NaCl, 21.4 mM $NaHCO_3$, 2.5 mM KCl, 1.2 mM NaH_2PO_4, 1.2 mM $MgCl_2$, 2.4 mM $CaCl_2$, 10 mM glucose) at 34°C for an additional 15 min. Slices were then kept at room temperature (20–24°C) for ≥45 min until use. A single slice was placed in the recording chamber where it was continuously superfused at a rate of 3–4 mL per min with oxygenated aCSF. Neurons were visualized with an upright microscope (SliceScope Pro 1000, Scientifica) equipped with infrared-differential interference contrast and fluorescence optics.

Electrically-evoked recordings—GABAergic transmission was recorded in whole-cell voltage-clamp mode, with membrane potential clamped at −70 mV using borosilicate glass microelectrodes (3–5 MΩ) filled with internal solution consisting of (in mM): 140 CsCl, 1 BAPTA, 10 HEPES, 5 $MgCl_2$, 5 Mg-ATP, 0.3 Na_2GTP, and 10 lidocaine *N*-ethyl bromide (QX-314), pH 7.35 and 290 mOsm. Glutamate receptor antagonists (1 mM kynurenate or 10 μM CNQX and 50 μM DAP-5) were used to isolate inhibitory postsynaptic currents (IPSCs). Electrically-evoked IPSCs were elicited by applying a pair (100 ms interstimulus interval;ISI) of 50 μs current pulses at 0.1 Hz through a bipolar tungsten electrode (resistance = 1 MΩ; WPI, Sarasota, FL) positioned 100-150 μm lateral to the patched neuron in the PVH. The intensity of the stimulation was adjusted so that the average IPSC

amplitude was ~75-80% of maximal amplitude for each recording and ranged from 50-600 μA. For pharmacological recordings (Fig 3), GDP-β-S was included in the pipette to block potential postsynaptic $GABA_B$ responses. The paired pulse ratio (PPR) of evoked IPSCs was calculated by dividing the mean peak amplitude of the second evoked response (A_2) by the mean peak amplitude of the first response (A_1) (PPR= mean A_2/ mean A_1) during the 2 min epoch prior to drug application and during the last 2 min of drug exposure. Drugs for pharmacology recordings: $GABA_B$ receptor agonist (baclofen, 30 μM; Tocris) and antagonists (saclofen, 200μM or CGP 52432,10 μM; Tocris); neuropeptide Y (NPY, 300 nM; Anaspec), and NPY receptor antagonists (NPY1 receptor: BIBO3304, 100 nM; NPY2 receptor: BIIE0246, 100 nM; NPY5 receptor: CGP71683, 100 nM; Tocris) were prepared and used according to manufacturer's specifications.

ChR2-assisted circuit mapping (CRACM)—In *vGAT*-IRES-Cre::*Crh*-IRES-FlpO::FLTG mice, CRH neurons in the PVH were genetically labeled with a Flp-dependent tdTomato tag (i.e. CRH--IRES-FlpO::tdTomato) and AAV9-EF1a-DIO-ChR2(H134R)-eYFP was expressed in the BNST. Open-tip resistances for patch pipettes were 3-5 MΩ and were backfilled with the same internal described in the previous section. Light-evoked IPSCs were isolated using glutamate receptor antagonists (1 mM kynurenate or 10 μM CNQX and 50 μM AP-5). To photostimulate ChR2-positive fibers, an LED light source was used (470 nm, Cool LED pE-100). The blue light was focused onto the back aperture of the microscope objective (40X) producing wide-field exposure around the recorded neuron of 10-15 mW per mm^2 as measured using an optical power meter (PM100D, Thorlabs). The light output was controlled by a programmable pulse stimulator (Master 8, A.M.P.I.) and pClamp 10.5 software (Axon Instruments). The light-evoked IPSC protocol consisted of four blue light pulses (470 nm wavelength, 2 ms duration) administered 1 s apart during the first 4 s of a 10-s sweep, repeated for a total of 30 sweeps. Evoked IPSCs with short latency (≤6 ms) upon light stimulation were considered as light-driven.

Analysis—All recordings were made using a Multiclamp 700B amplifier, and data were filtered at 2 kHz and digitized at 20 Hz. Access resistance (<30 MΩ) was continuously monitored by a voltage step and recordings were accepted for analysis if changes were <15%. All recordings were analyzed offline using Clampfit 10.5. eIPSC amplitude upon application of drugs was compared as follows: For onedrug experiments, baseline (3 minutes preceding drug application) and Drug (the last 3 minutes of the recording). For two-drug experiments (sequential NPY and Baclofen), baseline (2 minutes preceding drug application, first drug (the last 2 minutes of the recording prior to drug 2), and second drug (last 2 mins of the recording).

Single-cell RNA sequencing of analysis of PVH neurons

Previously published data from PVH neurons was obtained from the NCBI Gene Expression Omnibus database (GSE148568)[44]. Data were processed and analyzed in R using Seurat version 4[58]. The SCTransform function was used to scale, normalize, and identify variable genes. Principal component analysis on the 3,000 most variable genes was used for dimensionality reduction and cell clustering. Initial cell clustering identified two small non-neuronal clusters and one small cluster with low gene detection. These clusters were

subsequently removed and the remaining 766 PVH neurons were reclustered as above. Differential expression analysis across cell clusters was done with the Wilcoxon Rank Sum test to identify marker genes for putative PVH cell types and clusters were named based on previously reported marker genes[44].

Histology

Mice were terminally anesthetized with 7% choral hydrate (500 mg/kg; Sigma Aldrich) diluted in saline and transcardially perfused with 0.1 M phosphate-buffered saline (PBS) followed by 10% neutral-buffered formalin solution (NBF; Thermo Fisher Scientific). Extracted brains were post-fixed overnight at 4°C in NBF, cryoprotected in 20% sucrose, sectioned coronally at 30 μm on a freezing microtome (Leica Biosystems), and stored in cryoprotectant solution at −20°C until used for immunohistochemistry.

Immunohistochemistry—Brain sections were washed 3X in PBS prior to blocking (3% normal donkey serum and 0.4% Triton X-100 in PBS) for one hour at room temperature. Primary antibody was diluted in blocking solution and incubated overnight at room temperature. The following antibodies were used: Chicken anti-GFP (Invitrogen; 1:3000, A10262) and Goat anti-AgRP (Neuromics; 1:3000, GT15023). The following day the sections were washed 5X in PBS, then incubated for 2 hours at room temperature in donkey anti-chicken Alexa Fluor 488-conjugated secondary antibody (Jackson ImmunoResearch; 1:1000, 703-545-155) or donkey anti-goat Alexa Fluor 647 fluorescent secondary antibody (Invitrogen; 1:1000, A21447) prepared in blocking solution. Finally, sections were washed 3X in PBS, mounted on gelatin-coated slides, and coverslipped with VECTASHIELD® Antifade Mounting Medium, with DAPI (Vector Laboratories). Fluorescent images were taken using an Olympus VS120 slide-scanning microscope or a confocal microscope (Zeiss LSM 880). Fluorescent images were adjusted minimally for brightness and contrast using Olympus OlyVIA (3.4.1) and Image J (1.53c)

Data Analysis

Statistical analyses were performed using GraphPad Prism 8 software and are described in the figure legends. No statistical method was used to predetermine sample size, nor were randomization and blinding methods used. Statistical significance was defined as $p < 0.05$. All data presented met the assumptions of the statistical test employed. Experimental animals were excluded if histological validation revealed poor or absent reporter expression. N values reflect the final number of validated animals per group.

Extended Data

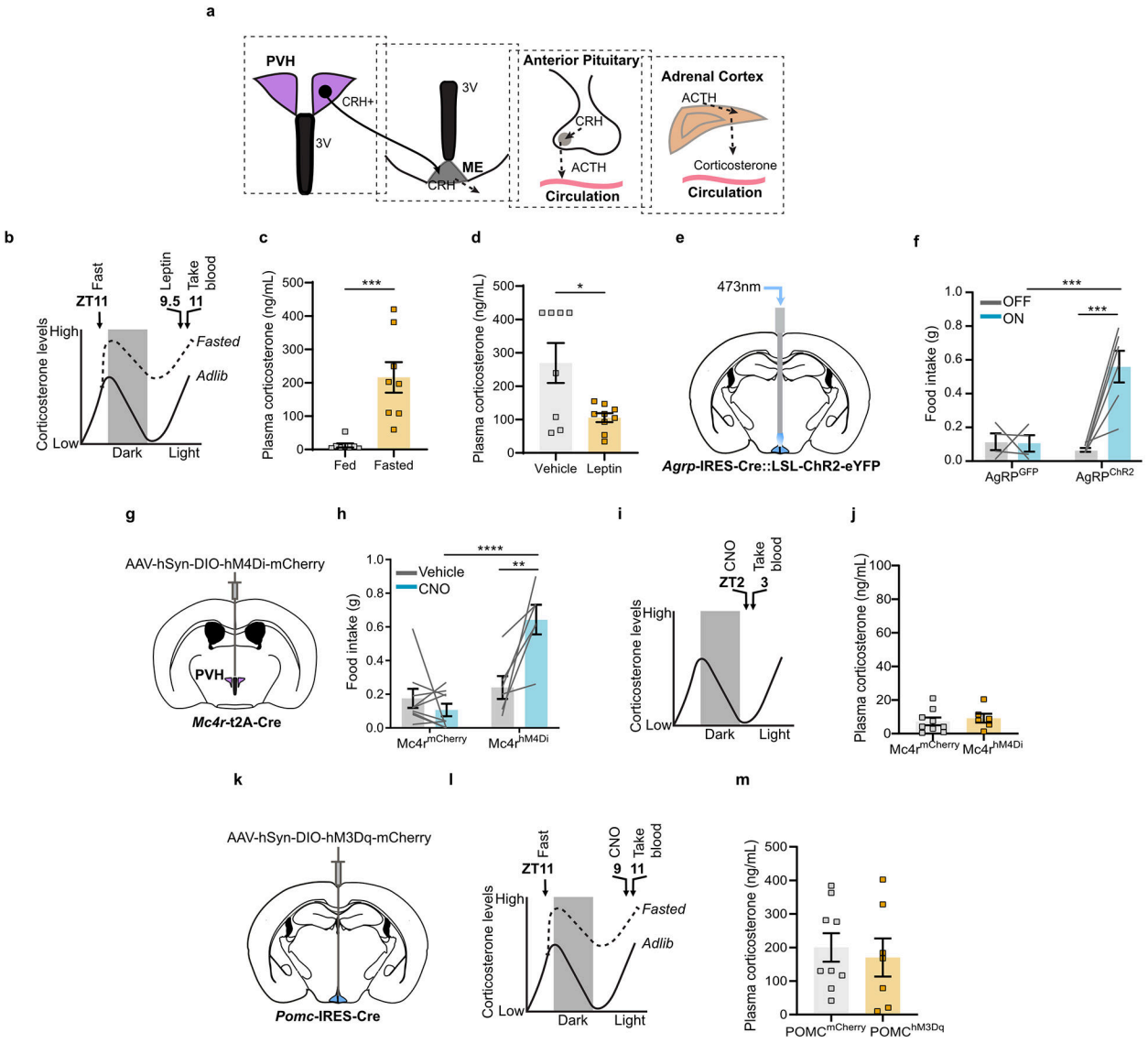

Extended Data Fig. 1. Fasting activation of the HPA axis is regulated by leptin but not by the arcuate PVH melanocortin system.

a, Scheme of the HPA axis. **b,** Time-line for leptin injection. **c,** Corticosterone levels were elevated in mice fasted for 24 hours compared to fed mice ($n = 8$ per group. Two-tailed unpaired *t*-test- ***$P = 0.0006$). **d,** I.P. administration of leptin reduced corticosterone levels in fasted mice ($n = 8$ vehicle, $n = 9$ leptin. Two-tailed unpaired *t*-test- *$P = 0.0130$). **e,** Schematic of optogenetic stimulation of AgRP neurons. **f,** One hour food intake by *Agrp*-IRES-Cre mice expressing ChR2 or GFP in the arcuate ($n = 4$ $AgRP^{GFP}$, $n = 6$ AgRPChR2. Two-way ANOVA; Sidak's multiple comparisons test. AgRPGFP ON vs. AgRPChR2 ON- ***$P = 0.0008$; AgRPChR2 OFF vs. AgRPChR2 ON- ***$P = 0.0001$). **g,** Schematic of Cre-dependent AAV-hM4Di-mCherry stereotaxic injection into the PVH of *Mc4r*-t2A-Cre mice. **h,** Three hour food intake by *Mc4r*-t2A-Cre mice expressing

hM4Di or mCherry in the PVH (n = 9 MC4RmCherry, n = 6 MC4RhM4Di. Two-way ANOVA; Sidak's multiple comparisons test. MC4RmCherry CNO vs. MC4RhM4Di CNO- ****P = <0.0001; MC4RhM4Di Vehicle vs. MC4RhM4Di CNO- **P = 0.0015). **i,** Time-line for chemogenetic inhibition of PVH*Mc4r* neurons. **j,** Inhibition of PVH^{Mc4r} neurons did not affect corticosterone in fed mice (n = 9 MC4RmCherry, n = 6 MC4RhM4Di. Two-tailed unpaired t-test- P = 0.5933). **k,** Schematic of Cre-dependent AAV-hM3Gq-mCherry stereotaxic injection into arcuate nucleus of *Pomc*-IRES-Cre mice. **l,** Time-line for chemogenetic activation of POMC neurons. **m,** Activation of POMC neurons did not affect corticosterone in fasted mice (n = 9 POMCmCherry, n = 7 POMChM3Gq. Two-tailed unpaired t-test- P = 0.6736). Scale bar = 200 μm. Data represent = mean ± sem.

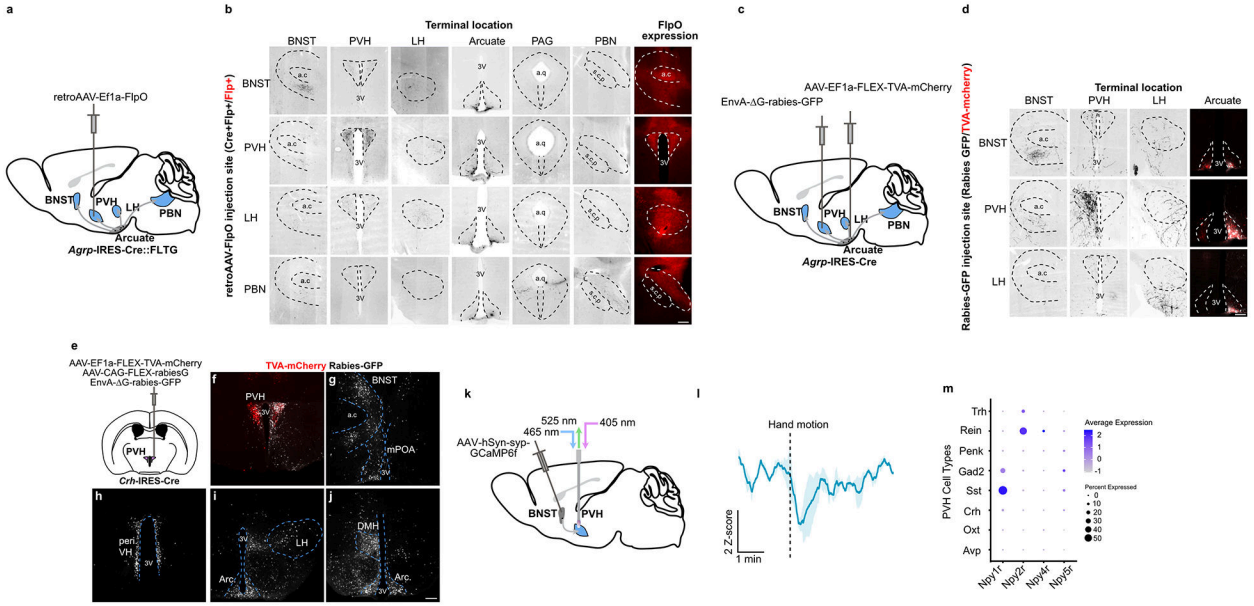

Extended Data Fig. 2. AgRP neuron collaterals and characterization of GABAergic afferents to PVH*Crh* neurons.

a, Schematic of collateral mapping via injection of retro-AAV-FlpO into *Agrp*-IRES-Cre::FLTG mice. **b,** AgRP neuron terminals detected upon injection of retro-AAV-FlpO into individual AgRP neuron efferent sites (denoted by row headings) in *Agrp*-IRES-Cre::FLTG mice. a.c: anterior commissure, 3V: third ventricle, a.q: aqueduct, s.c.p: superior cerebellar peduncle. **c,** Schematic of rabies-based collateral mapping. EnvA pseudotyped rabies-ΔG-GFP was injected into AgRP neuron terminal areas (PVH example) in *Agrp*-IRES-Cre mice that were previously injected with AAV-FLEX-TVA-mCherry in the arcuate. **d,** AgRP neuron terminals detected upon injection of EnvA pseudotyped rabies-ΔG-GFP into individual AgRP neuron efferent sites (denoted by row headings) in *Agrp*-IRES-Cre mice. **e,** Schematic of monosynaptic rabies mapping from PVH*Crh* neurons. **f-j,** Representative images of starter cells and putative afferents containing rabies-GFP labeled neurons in the PVH (**f**), BNST and mPOA (**g**), periventricular hypothalamus (**h**), LH and anterior arcuate nucleus (**i**) and DMH and posterior arcuate nucleus (**j**). PVH: paraventricular hypothalamus, a.c: anterior commissure, BNST: bed nucleus of the stria terminalis, mPOA: medial preoptic area, 3V: Third ventricle, peri VH: periventricular hypothalamus, LH: lateral hypothalamus,

Arc: arcuate nucleus, DMH: dorsomedial hypothalamus. **k,** Schematic of recordings of BNST→PVH terminals. These mice are those used in Fig. 5j-o. **l,** BNST→PVH axons reduced activity in response to a looming hand motion stimulus over the animal (n = 3 mice). **m,** Expression of NPYRs in major PVH neuron cell types derived from single-cell RNA sequencing of PVH neurons43, plotted as average normalized expression level and fraction of cells in each cluster that express the receptor. Scale bar = 200 μm. Data represent = mean ± sem.

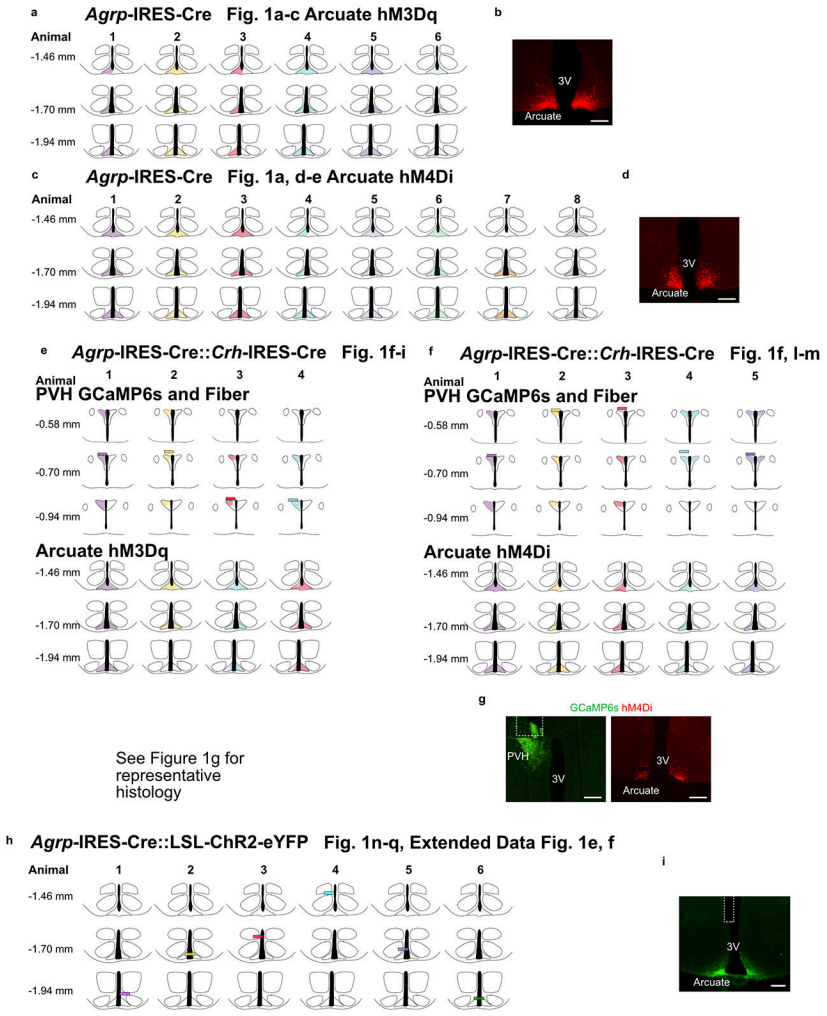

Extended Data Fig. 3. Schematic of AAV spread in *Agrp*-IRES-Cre mice, AAV spread and fiber placements in *Agrp*-IRES-Cre::*Crh*-IRES-Cre mice and fiber placements in *Agrp*-IRES-Cre::LSL-ChR2-eYFP mice.

a, Schematics representing AAV spread (shaded regions) for every animal related to experiments in Fig. 1a-c. Each animal is represented by a different colour. **b,** Representative image of hM3Dq-mCherry expression in AgRP neuron somas in the arcuate nucleus. **c,** Schematics representing AAV spread (shaded regions) for every animal related to experiments in Fig. 1a, d-e. **d,** Representative image of hM4Di-mCherry expression in AgRP neuron somas in the arcuate nucleus. Each animal is represented by a different colour. **e,** Schematics representing AAV spread (shaded regions) and fiber placement (rectangles) for

every animal related to experiments in Fig. 1f-i. Each animal is represented by a different colour. See Fig. 1g for a representative histological image. **f,** Schematics representing AAV spread (shaded regions) and fiber placement (rectangles) for every animal related to experiments in Fig. 1f, l-m. **g,** Representative images of GCaMP6s expression in PVH*Crh* neurons, optic fiber placement in the PVH and hM4Di-mCherry expression in AgRP neuron somas in the arcuate nucleus. Each animal is represented by a different colour. **h,** Schematics representing fiber placements (rectangles) for every animal related to experiments in Fig. 1n-q and Extended Data Fig. 1e, f. Each animal is represented by a different colour. **i,** Representative image of ChR2-eYFP expression in AgRP neuron somas in the arcuate nucleus and fiber placement. Scale bar = 200 μm. 3V = Third ventricle. The schematics were created using The Mouse Brain in Stereotaxic Coordinates Second Edition (Paxinos and Franklin).

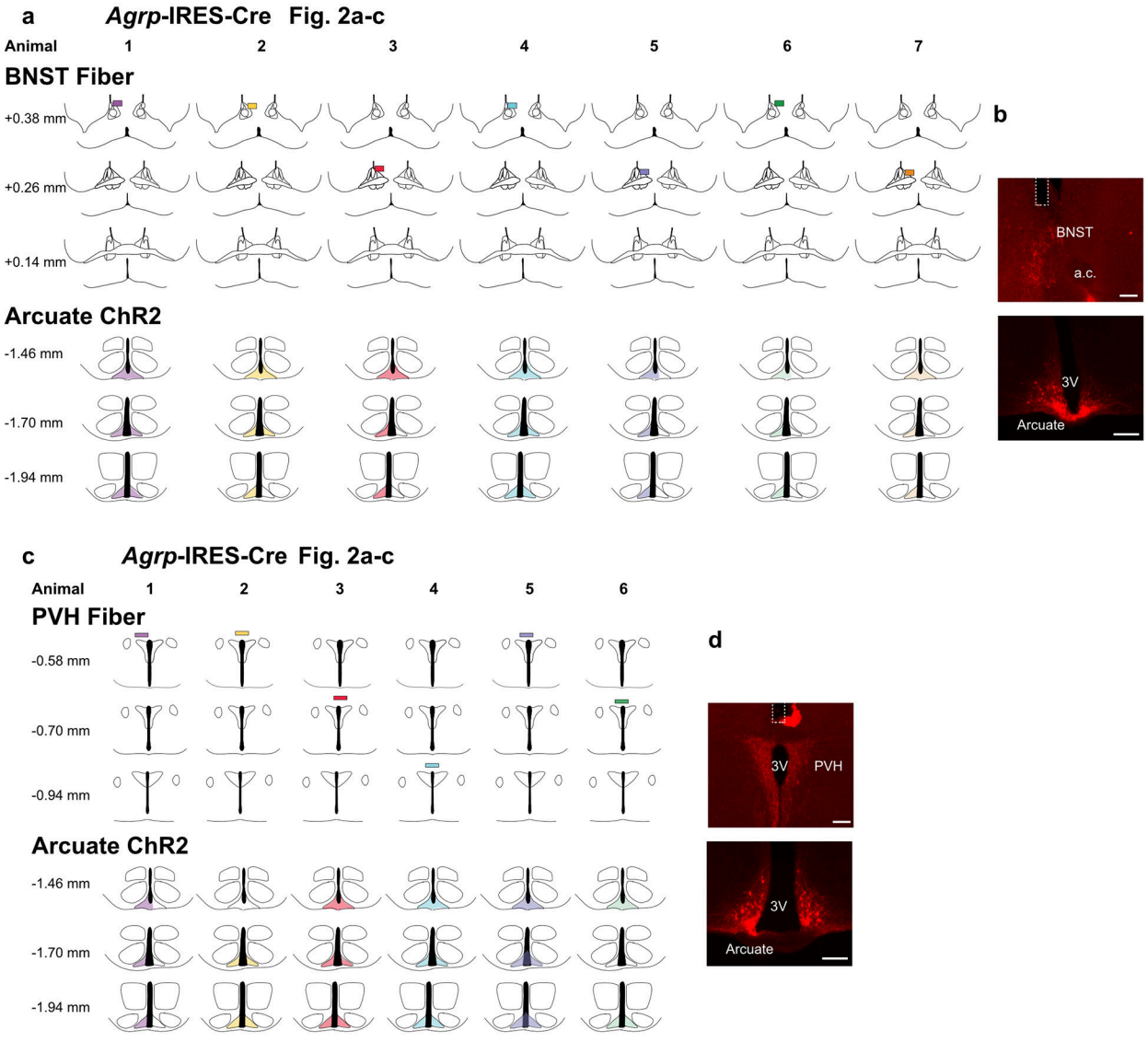

Extended Data Fig. 4. Schematic of AAV spread and fiber placements in *Agrp*-IRES-Cre mice.

a, Schematics representing AAV spread (shaded regions) and fiber placements (rectangles) for every animal related to experiments in Fig. 2a-c. Each animal is represented by a different colour. **b,** Representative images of ChR2-mCherry expression in AgRP neuron somas in the arcuate nucleus and fiber placement in the BNST. **c,** Schematics representing AAV spread (shaded regions) and fiber placements (rectangles) for every animal related to experiments in Fig. 2a-c. Each animal is represented by a different colour. **d,** Representative images of ChR2-mCherry expression in AgRP neuron somas in the arcuate nucleus and fiber placement in the PVH. Scale bar = 200 μm. 3V = Third ventricle. a.c. = anterior commisure. The schematics were created using The Mouse Brain in Stereotaxic Coordinates Second Edition (Paxinos and Franklin).

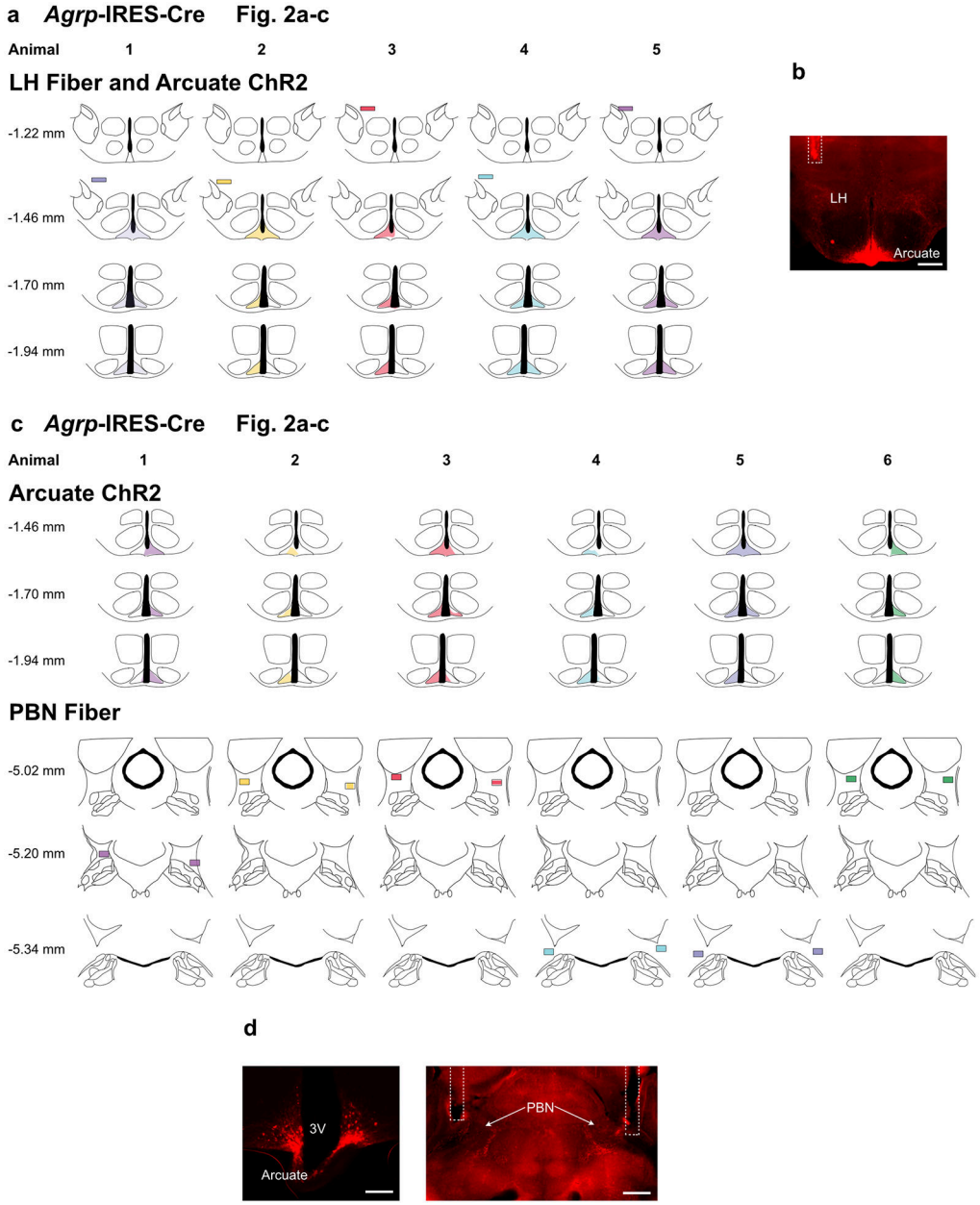

Extended Data Fig. 5. Schematic of AAV spread and fiber placements in *Agrp*-IRES-Cre mice. **a,** Schematics representing AAV spread (shaded regions) and fiber placements (rectangles) for every animal related to experiments in Fig. 2a-c. Each animal is represented by a different colour. **b,** Representative image of ChR2-mCherry expression in AgRP neuron somas in the arcuate nucleus and fiber placement in the LH. Scale bar = 500 μm. **c,** Schematics representing AAV spread (shaded regions) and fiber placements (rectangles) for every animal related to experiments in Fig. 2a-c. Each animal is represented by a different colour. **d,** Representative images of ChR2-mCherry expression in AgRP neuron somas in the arcuate nucleus and fiber placement in the PBN. Left scale bar = 200 μm, Right scale bar = 500 μm. 3V = Third ventricle. The schematics were created using The Mouse Brain in Stereotaxic Coordinates Second Edition (Paxinos and Franklin).

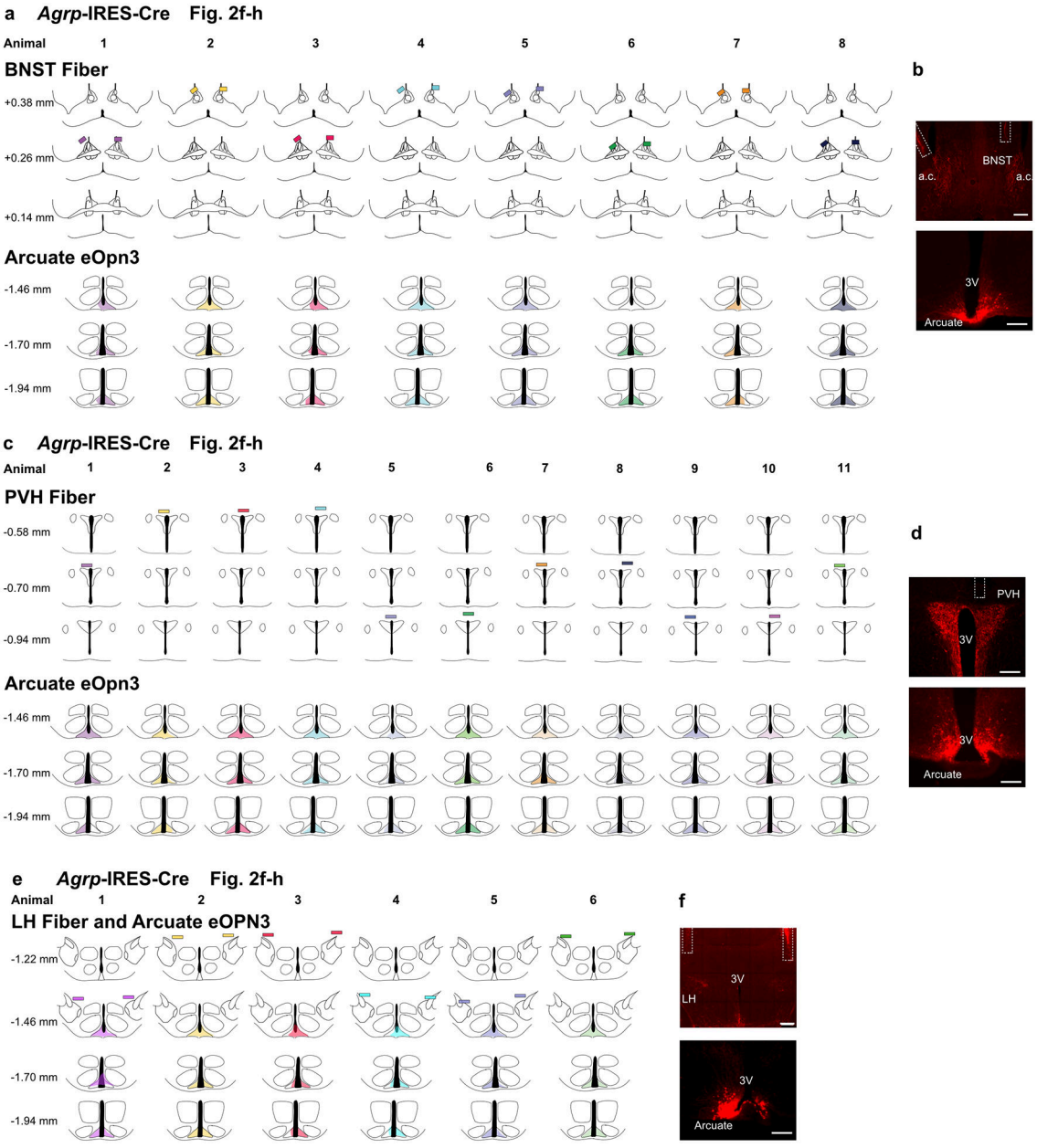

Extended Data Fig. 6. Schematic of AAV spread and fiber placements in *Agrp*-IRES-Cre mice.

a, Schematics representing AAV spread (shaded regions) and fiber placements (rectangles) for every animal related to experiments in Fig. 2f-h. Each animal is represented by a different colour. **b,** Representative images of eOpn3-mScarlet expression in AgRP neuron somas in the arcuate nucleus and fiber placement in the BNST. **c,** Schematics representing AAV spread (shaded regions) and fiber placements (rectangles) for every animal related to experiments in Fig. 2f-h. Each animal is represented by a different colour. **d,** Representative images of eOpn3-mScarlet expression in AgRP neuron somas in the arcuate nucleus and fiber placement in the PVH. **e,** Schematics representing AAV spread (shaded regions) and fiber placements (rectangles) for every animal related to experiments in Fig. 2f-h. Each animal is represented by a different colour. **f,** Representative images of eOpn3-mScarlet

expression in AgRP neuron somas in the arcuate nucleus and fiber placement in the LH. Scale bar = 200 μm. 3V = Third ventricle. a.c. = anterior commisure. The schematics were created using The Mouse Brain in Stereotaxic Coordinates Second Edition (Paxinos and Franklin).

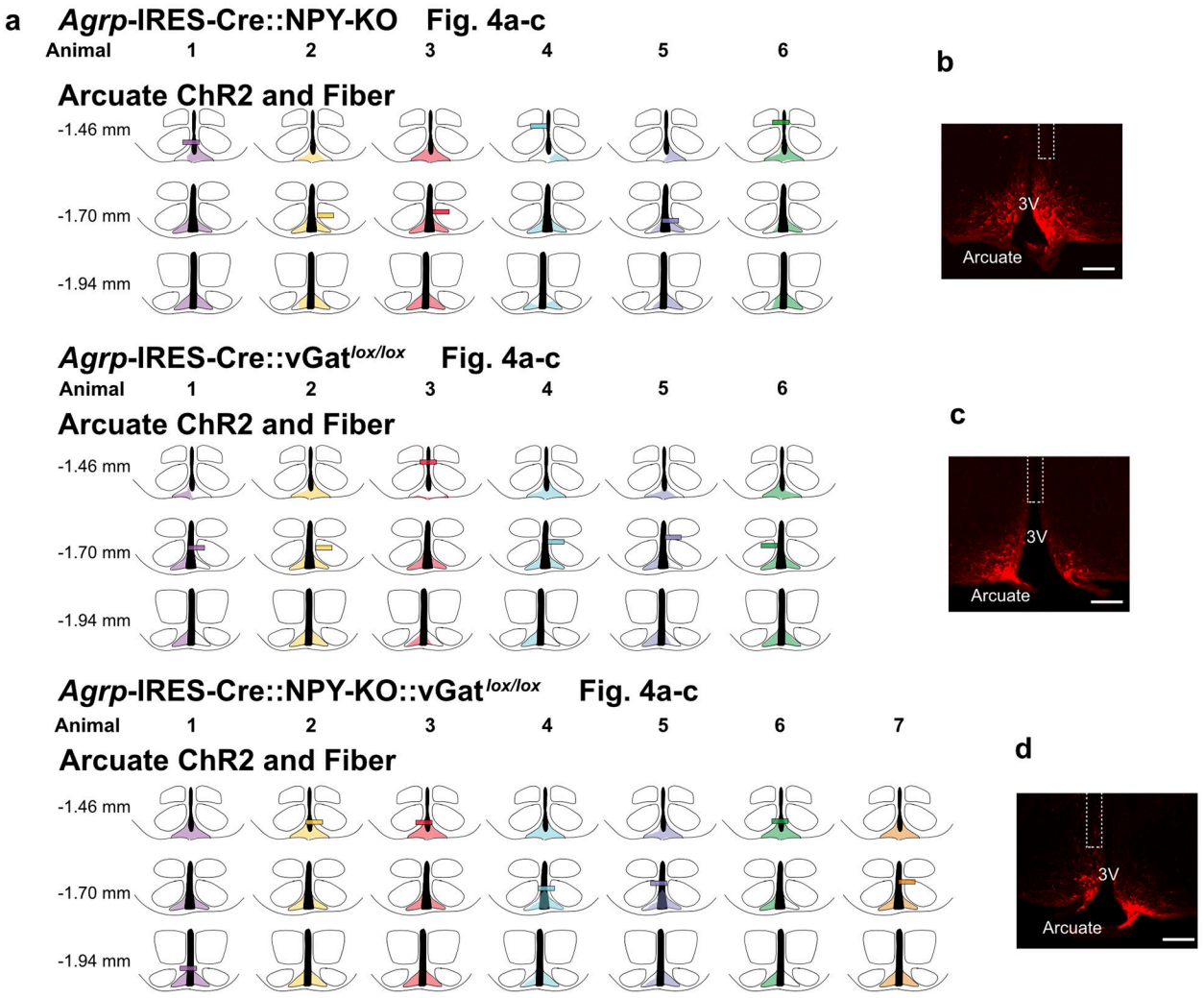

Extended Data Fig. 7. Schematic of AAV spread and fiber placements in *Agrp*-IRES-Cre::NPY-KO, *Agrp*-IRES-Cre::vGat$^{lox/lox}$ and *Agrp*-IRES-Cre::NPY-KO::vGat$^{lox/lox}$ mice.

a, Schematics representing AAV spread (shaded regions) and fiber placements (rectangles) for every animal related to experiments in Fig. 4a-c. Each animal is represented by a different colour. **b-d.** Representative images of ChR2-mCherry expression in AgRP neuron somas and fiber placement in the arcuate nucleus. Scale bar = 200 μm. 3V = Third ventricle. The schematics were created using The Mouse Brain in Stereotaxic Coordinates Second Edition (Paxinos and Franklin).

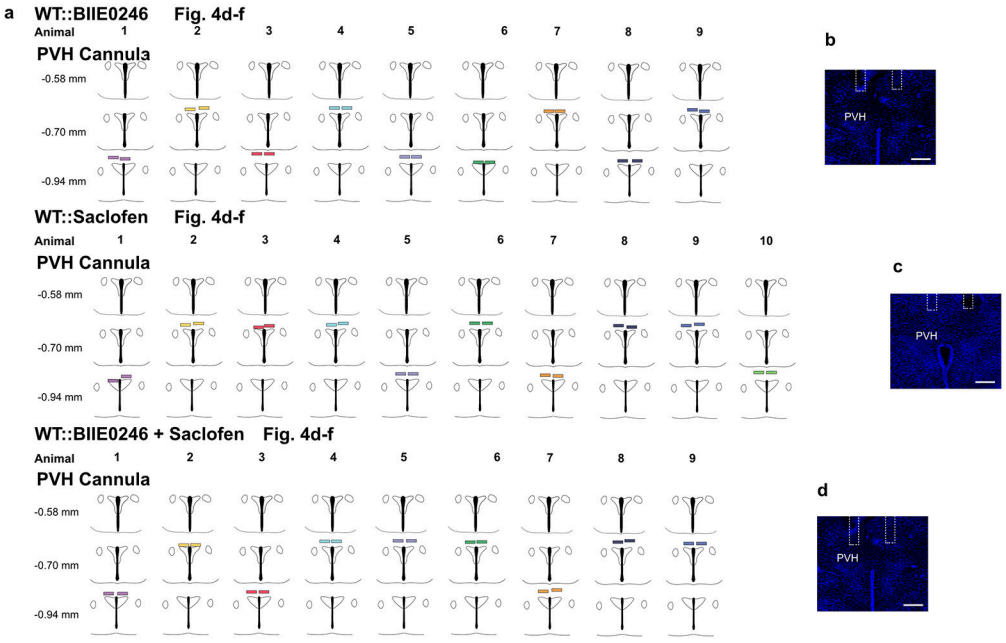

Extended Data Fig. 8. Schematic of infusion cannula placements in WT mice.

a, Schematics representing infusion cannula placements (rectangles) for every animal related to experiments in Fig. 4d-f. Each animal is represented by a different colour. **b-d,** Representative images of cannula placement above the PVH. Scale bar = 200 μm. The schematics were created using The Mouse Brain in Stereotaxic Coordinates Second Edition (Paxinos and Franklin).

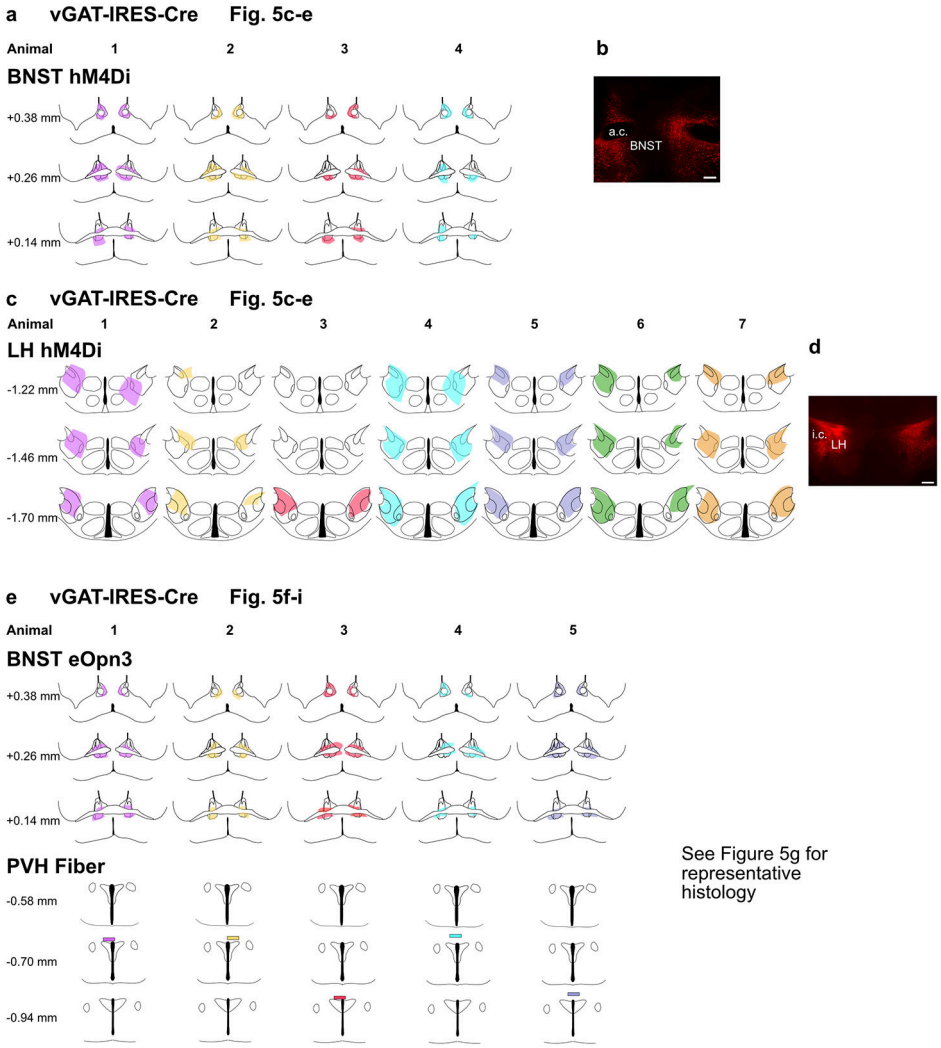

Extended Data Fig. 9. Schematic of AAV spread and fiber placements in vGAT-IRES-Cre mice.

a, Schematics representing AAV spread (shaded regions) for every animal related to experiments in Fig. 5c-e. Each animal is represented by a different colour. **b,** Representative image of hM4Di-mCherry expression in BNSTvGAT neuron somas. **c,** Schematics representing AAV spread (shaded regions) for every animal related to experiments in Fig. 5c-e. Each animal is represented by a different colour. **d,** Representative image of hM4Di-mCherry expression in LHvGAT neuron somas. **e,** Schematics representing AAV spread (shaded regions) and fiber placements (rectangles) for every animal related to experiments in Fig. 5f-i. Each animal is represented by a different colour. See Fig. 5g for a representative histological image. Scale bar = 200 μm. a.c. = anterior commisure, i.c. = internal capsule. The schematics were created using The Mouse Brain in Stereotaxic Coordinates Second Edition (Paxinos and Franklin).

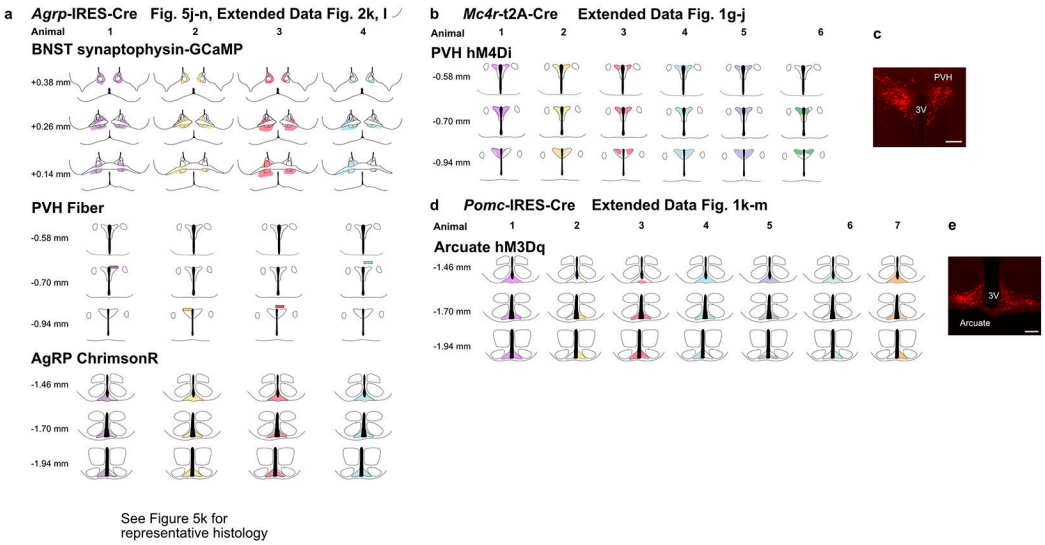

Extended Data Fig. 10. Schematic of AAV spread and fiber placements in *Agrp*-IRES-Cre mice, *Mc4r*-IRES-Cre and *Pomc*-IRES-Cre mice.

a, Schematics representing AAV spread (shaded regions) and fiber placements (rectangles) for every animal related to experiments in Fig. 5j-n and Extended Data Fig. 2k, l. Each animal is represented by a different colour. See Fig. 5k for a representative histological image. **b,** Schematics representing AAV spread (shaded regions) for every animal related to experiments in Extended Data Fig. 1g-j. Each animal is represented by a different colour. **c,** Representative image of hM4Di-mCherry expression in PVH^{Mc4r} neuron somas. **d,** Schematics representing AAV spread (shaded regions) for every animal related to experiments in Extended Data Fig. 1k-m. Each animal is represented by a different colour. **e,** Representative image of hM3Dq-mCherry expression in POMC neuron somas in the arcuate nucleus. Scale bar = 200 μm. 3V = Third ventricle. The schematics were created using The Mouse Brain in Stereotaxic Coordinates Second Edition (Paxinos and Franklin).

Acknowledgements

We thank Mark Andermann, Joe Majzoub and the Lowell laboratory for helpful discussions; Jia Yu, Chen Wu and Yanfang Li for technical assistance; Steve Liberles for providing the NPY-KO mice; and the Brigham Assay Core for running the ACTH radioimmunoassay. The confocal imaging was performed at BIDMC's Confocal Imaging Core. This work was supported by the NIH (P30DK046200, R01DK122976, R01DK075632, R01DK089044, R01DK111401, R01DK096010 to B.B.L and R00HL144923 to J.M.R). A.M.D was supported the Charles A. King Trust Postdoctoral Research Fellowship Program. H.K. was supported by a BBRF Young Investigator Grant.

Data Availability

Fiber photometry data reported in this study is available from:https://research.bidmc.harvard.edu/datashare/DataShareInfo.ASP?Submit=Display&ID=9. Source data are provided with this paper.

Code Availability

The custom analysis code used in this study is available on Github.(https://github.com/AMDouglass/Douglass_Resch_Madara_etal)

References

1. Ahima RS et al. Role of leptin in the neuroendocrine response to fasting. Nature 382, 250–252 (1996). [PubMed: 8717038]
2. Dallman MF et al. Starvation: Early Signals, Sensors, and Sequelae. Endocrinology 140, 4015–4023 (1999). [PubMed: 10465271]
3. Perry RJ et al. Leptin Mediates a Glucose-Fatty Acid Cycle to Maintain Glucose Homeostasis in Starvation. Cell 172, 234–236.e17 (2018). [PubMed: 29307489]
4. Muglia L, Jacobson L, Dikkest P & Majzoub JA Corticotropin-releasing hormone deficiency reveals major fetal but not adult glucocorticoid need. Nature 373, 427–432 (1995). [PubMed: 7830793]
5. Steinhauser ML et al. The circulating metabolome of human starvation. JCI Insight 3, e121434 (2018). [PubMed: 30135314]
6. Long CNH, Katzin B & Fry EG The adrenal cortex and carbohydrate metabolism. Endocrinology 26, 309–344 (1940).
7. Chihaoui M. et al. The risk for hypoglycemia during Ramadan fasting in patients with adrenal insufficiency. Nutrition 45, 99–103 (2018). [PubMed: 29129244]
8. Exton J. Regulation of gluconeogenesis by glucocorticoids. Monogr Endocrinol 12, 535–46 (1979). [PubMed: 386091]
9. Kuo T, McQueen A, Chen TC & Wang JC Regulation of Glucose Homeostasis by Glucocorticoids. Adv. Exp. Med. Biol 872, 99 (2015). [PubMed: 26215992]
10. Goldberg AL, Tischler M, DeMartino G, G. G. Hormonal regulation of protein degradation and synthesis in skeletal muscle. Fed Proc 39, 31–6 (1980). [PubMed: 7351242]
11. Djurhuus CB et al. Effects of cortisol on lipolysis and regional interstitial glycerol levels in humans. Am. J. Physiol. - Endocrinol. Metab 283, 46–1 (2002).
12. Aponte Y, Atasoy D & Sternson SM AGRP neurons are sufficient to orchestrate feeding behavior rapidly and without training. Nat. Neurosci 14, 351–355 (2011). [PubMed: 21209617]
13. Krashes MJ et al. Rapid, reversible activation of AgRP neurons drives feeding behavior in mice. J. Clin. Invest 121, 1424–8 (2011). [PubMed: 21364278]
14. Livneh Y. et al. Homeostatic circuits selectively gate food cue responses in insular cortex. Nature 546, 611–616 (2017). [PubMed: 28614299]
15. Fernandes ACA et al. Arcuate AgRP, but not POMC neurons, modulate paraventricular CRF synthesis and release in response to fasting. Cell Biosci. 12, 1–14 (2022). [PubMed: 34980273]
16. Spencer RL & Deak T A users guide to HPA axis research. Physiology and Behavior 178, 43–65 (2017). [PubMed: 27871862]
17. Betley JN, Cao ZFH, Ritola KD & Sternson SM Parallel, redundant circuit organization for homeostatic control of feeding behavior. Cell 155, 1337–50 (2013). [PubMed: 24315102]
18. Betley JN et al. Neurons for hunger and thirst transmit a negative-valence teaching signal. Nature 521, 180–185 (2015). [PubMed: 25915020]
19. Garfield AS et al. A neural basis for melanocortin-4 receptor–regulated appetite. Nat. Neurosci 18, 863–871 (2015). [PubMed: 25915476]
20. Mahn M. et al. Efficient optogenetic silencing of neurotransmitter release with a mosquito rhodopsin. Neuron 109, 1621–1635.e8 (2021). [PubMed: 33979634]
21. Ziegler DR, Cullinan WE & Herman JP Distribution of vesicular glutamate transporter mRNA in rat hypothalamus. J. Comp. Neurol 448, 217–229 (2002). [PubMed: 12115705]
22. Cowley MA et al. Integration of npy, agrp, and melanocortin signals in the hypothalamic paraventricular nucleus: Evidence of a cellular basis for the adipostat. Neuron 24, 155–163 (1999). [PubMed: 10677034]
23. Pronchuk N, Beck-Sickinger AG & Colmers WF Multiple NPY receptors inhibit GABAA synaptic responses of rat medial parvocellular effector neurons in the hypothalamic paraventricular nucleus. Endocrinology 143, 535–543 (2002). [PubMed: 11796508]
24. Mackay JP et al. NPY2 receptors reduce tonic action potential-independent gabab currents in the basolateral amygdala. J. Neurosci 39, 4909–4930 (2019). [PubMed: 30971438]

25. Colmers PLW & Bains JS Balancing tonic and phasic inhibition in hypothalamic corticotropin-releasing hormone neurons. J. Physiol 596, 1919–1929 (2018). [PubMed: 29419884]
26. Krashes MJ, Shah BP, Koda S & Lowell BB Rapid versus delayed stimulation of feeding by the endogenously released AgRP neuron mediators GABA, NPY, and AgRP. Cell Metab. 18, 588–95 (2013). [PubMed: 24093681]
27. Wahlestedt C. et al. Neuropeptide Y (NPY) in the area of the hypothalamic paraventricular nucleus activates the pituitary-adrenocortical axis in the rat. Brain Res. 417, 33–38 (1987). [PubMed: 3040184]
28. Johnson CS, Bains JS & Watts AG Neurotransmitter diversity in pre-synaptic terminals located in the parvicellular neuroendocrine paraventricular nucleus of the rat and mouse hypothalamus. J. Comp. Neurol 526, 1287–1306 (2018). [PubMed: 29424419]
29. Cole RL & Sawchenko PE Neurotransmitter regulation of cellular activation and neuropeptide gene expression in the paraventricular nucleus of the hypothalamus. J. Neurosci 22, 959–969 (2002). [PubMed: 11826124]
30. Roland BL & Sawchenko PE Local origins of some GABAergic projections to the paraventricular and supraoptic nuclei of the hypothalamus in the rat. J. Comp. Neurol 332, 123–143 (1993). [PubMed: 7685780]
31. Cullinan WE, Ziegler DR & Herman JP Functional role of local GABAergic influences on the HPA axis. Brain Structure and Function 213, 63–72 (2008). [PubMed: 18696110]
32. Johnson SB et al. A Basal Forebrain Site Coordinates the Modulation of Endocrine and Behavioral Stress Responses via Divergent Neural Pathways. J. Neurosci 36, 8687–8699 (2016). [PubMed: 27535914]
33. Radley JJ, Gosselink KL & Sawchenko PE A Discrete GABAergic Relay Mediates Medial Prefrontal Cortical Inhibition of the Neuroendocrine Stress Response. J. Neurosci 29, 7330–7340 (2009). [PubMed: 19494154]
34. Michel MC et al. XVI. International Union of Pharmacology Recommendations for the Nomenclature of Neuropeptide Y, Peptide YY, and Pancreatic Polypeptide Receptors. Pharmacol. Rev 50, (1998).
35. Woodward CJH, Hervey GR, Oakey RE & Whitaker EM The effects of fasting on plasma corticosterone kinetics in rats. Br. J. Nutr 66, 117–127 (1991). [PubMed: 1931899]
36. Chen Y. et al. Sustained NPY signaling enables AgRP neurons to drive feeding. Elife 8, (2019).
37. Wahlestedt C, Hakanson R, Vaz CA & Zukowska-Grojec Z Norepinephrine and neuropeptide Y: vasoconstrictor cooperation in vivo and in vitro. Am. J. Physiol. Integr. Comp. Physiol 258, (1990).
38. Khan AM et al. MAP Kinases Couple Hindbrain-Derived Catecholamine Signals to Hypothalamic Adrenocortical Control Mechanisms during Glycemia-Related Challenges. J. Neurosci 31, 18479–18491 (2011). [PubMed: 22171049]
39. Atasoy D, Betley JN, Su HH & Sternson SM Deconstruction of a neural circuit for hunger. Nature 488, 172–177 (2012). [PubMed: 22801496]
40. Padilla SL et al. Agouti-related peptide neural circuits mediate adaptive behaviors in the starved state. Nat. Neurosci 19, 734–741 (2016). [PubMed: 27019015]
41. Li MM et al. The Paraventricular Hypothalamus Regulates Satiety and Prevents Obesity via Two Genetically Distinct Circuits. Neuron 102, 653–667.e6 (2019). [PubMed: 30879785]
42. Baur R & Sigel E On high- and low-affinity agonist sites in GABAA receptors. J. Neurochem 87, 325–332 (2003). [PubMed: 14511110]
43. Hill DR & Bowery NG 3H-baclofen and 3H-GABA bind to bicuculline-insensitive GABAB sites in rat brain. Nat. 1981 2905802 290, 149–152 (1981).
44. Xu S. et al. Behavioral state coding by molecularly defined paraventricular hypothalamic cell type ensembles. Science (80-.). 370, (2020).
45. Atasoy D. et al. A genetically specified connectomics approach applied to long-range feeding regulatory circuits. Nat. Neurosci. 2014 1712 17, 1830–1839 (2014).
46. Perry RJ et al. Leptin's hunger-suppressing effects are mediated by the hypothalamic–pituitary–adrenocortical axis in rodents. Proc. Natl. Acad. Sci. U. S. A 116, 13670–13679 (2019). [PubMed: 31213533]

47. Tong Q, Ye CP, Jones JE, Elmquist JK & Lowell BB Synaptic release of GABA by AgRP neurons is required for normal regulation of energy balance. Nat. Neurosci. 2008 119 11, 998–1000 (2008).

48. Krashes MJ et al. An excitatory paraventricular nucleus to AgRP neuron circuit that drives hunger. Nature 507, 238–242 (2014). [PubMed: 24487620]

49. Fenselau H. et al. A rapidly acting glutamatergic ARC→PVH satiety circuit postsynaptically regulated by α-MSH. Nat. Neurosci. 2016 201 20, 42–51 (2016).

50. Vong L. et al. Leptin Action on GABAergic Neurons Prevents Obesity and Reduces Inhibitory Tone to POMC Neurons. Neuron 71, 142–154 (2011). [PubMed: 21745644]

51. Madisen L. et al. A toolbox of Cre-dependent optogenetic transgenic mice for light-induced activation and silencing. Nat. Neurosci. 2012 155 15, 793–802 (2012).

52. Plummer NW et al. Expanding the power of recombinase-based labeling to uncover cellular diversity. Dev. 142, 4385–4393 (2015).

53. Erickson C, Clegg KE & Palmiter RD Sensitivity to leptin and susceptibility to seizures of mice lacking neuropeptide Y. Nat. 1996 3816581 381, 415–418 (1996).

54. Harms KJ, Tovar KR & Craig AM Synapse-Specific Regulation of AMPA Receptor Subunit Composition by Activity. J. Neurosci 25, 6379–6388 (2005). [PubMed: 16000628]

55. Chen TW et al. Ultrasensitive fluorescent proteins for imaging neuronal activity. Nat. 2013 4997458 499, 295–300 (2013).

56. Atasoy D, Aponte Y, Su HH & Sternson SM A FLEX Switch Targets Channelrhodopsin-2 to Multiple Cell Types for Imaging and Long-Range Circuit Mapping. J. Neurosci 28, 7025–7030 (2008). [PubMed: 18614669]

57. Akam T & Walton ME pyPhotometry: Open source Python based hardware and software for fiber photometry data acquisition. Sci. Rep 9, 1–11 (2019). [PubMed: 30626917]

58. Hao Y. et al. Integrated analysis of multimodal single-cell data. Cell 184, 3573–3587.e29 (2021). [PubMed: 34062119]

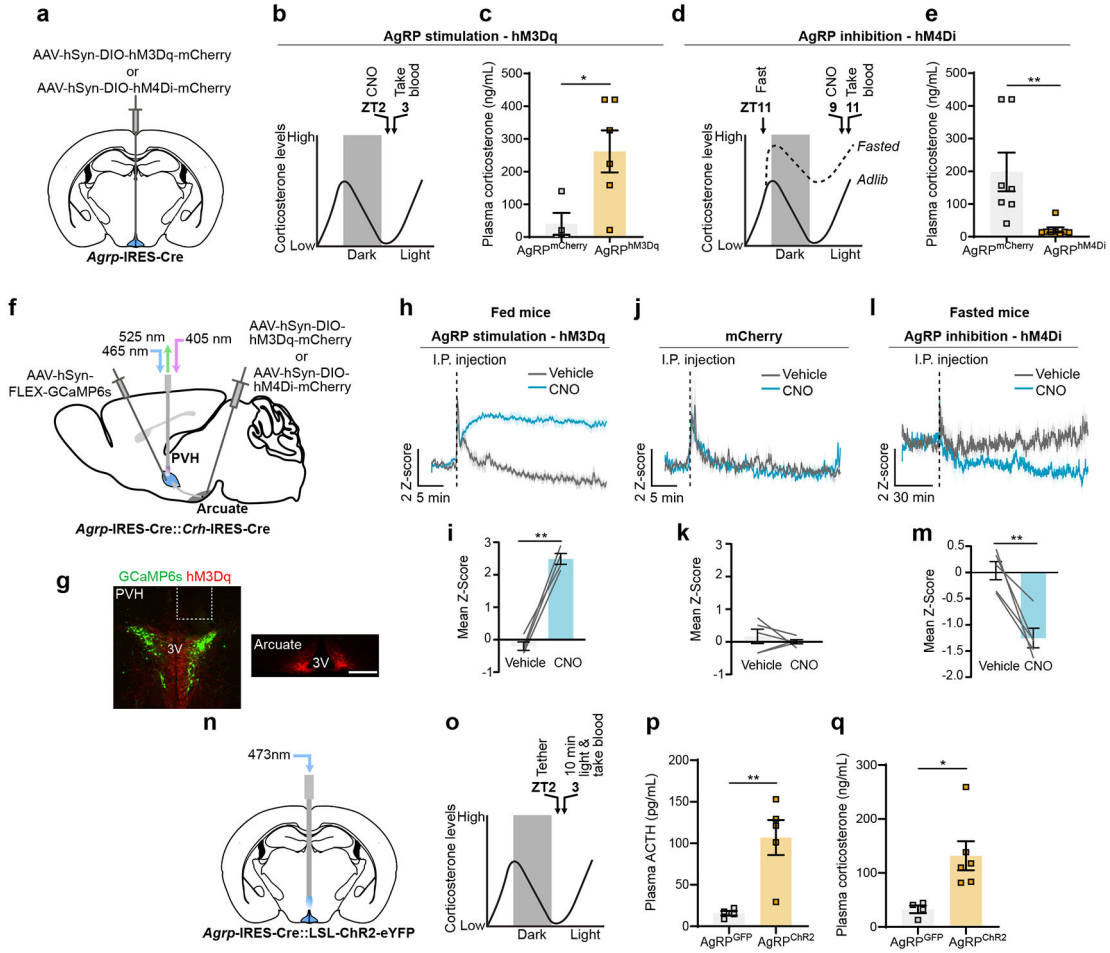

Figure 1. AgRP neurons drive the HPA axis during fasting.

a, Schematic of Cre-dependent AAV-hM3Dq-mcherry or hM4Di-mCherry injection into the arcuate of *Agrp*-IRES-Cre mice. **b,** Time-line for chemogenetic activation of AgRP neurons. **c,** AgRP neuron stimulation increased corticosterone in fed mice ($n = 4$ $AgRP^{mCherry}$, $n = 6$ $AgRP^{hM3Dq}$. Two-tailed unpaired *t*-test- *P = 0.0309). **d,** Time-line for chemogenetic inhibition of AgRP neurons. **e,** AgRP neuron inhibition reduced fasting corticosterone ($n = 7$ $Agrp^{mCherry}$, $n = 8$ $Agrp^{hM4Di}$. Two-tailed unpaired *t*-test- $^{**}P = 0.0076$). **f,** Schematic of photometry from PVH^{Crh} neurons and activation of AgRP neurons. **g,** Representative images of GCaMP6s expression in PVH^{Crh} neurons and hM3Dq-mCherry expression in AgRP neuron somas and terminals. **h,** Chemogenetic activation of AgRP neurons increased PVH^{Crh} neuron activity ($n = 4$ mice). **i,** Mean Ca^{2+} signal from PVH^{Crh} neurons after injection of CNO vs. vehicle ($n = 4$ mice. Two-tailed paired *t*-test- $^{**}P = 0.0012$). **j,** Injection of vehicle or CNO did not affect Ca2+ signal in PVH^{Crh} neurons in mCherry-expressing mice ($n = 5$ mice). **k,** Mean Ca^{2+} signal from PVH^{Crh} neurons after injection of CNO vs. vehicle ($n = 5$ mice. Two-tailed paired *t*-test- $P = 0.5297$). **l,** Chemogenetic inhibition of AgRP neurons reduced PVH^{Crh} neuron activity ($n = 5$ mice). **m,** Mean Ca^{2+} signal from PVH^{Crh} neurons after injection of CNO vs. vehicle ($n = 5$ mice. Two-tailed paired *t*-test- $^{**}P = 0.0071$). **n,** Schematic of optogenetic stimulation of AgRP neurons. **o,** Time-line for optogenetic stimulation of AgRP neurons. **p, q,** Optogenetic stimulation of

AgRP neurons increased ACTH ($n = 4$ AgRP^{GFP}, $n = 5$ AgRP^{ChR2}. Two-tailed unpaired t-test- $^{**}P = 0.0068$) (**p**) and corticosterone ($n = 4$ AgRP^{GFP}, $n = 6$ AgRP^{ChR2}, two-tailed unpaired t-test- $^{**}P = 0.0198$) (**q**). Scale bar = 200 μm. Data represent = mean ± sem.

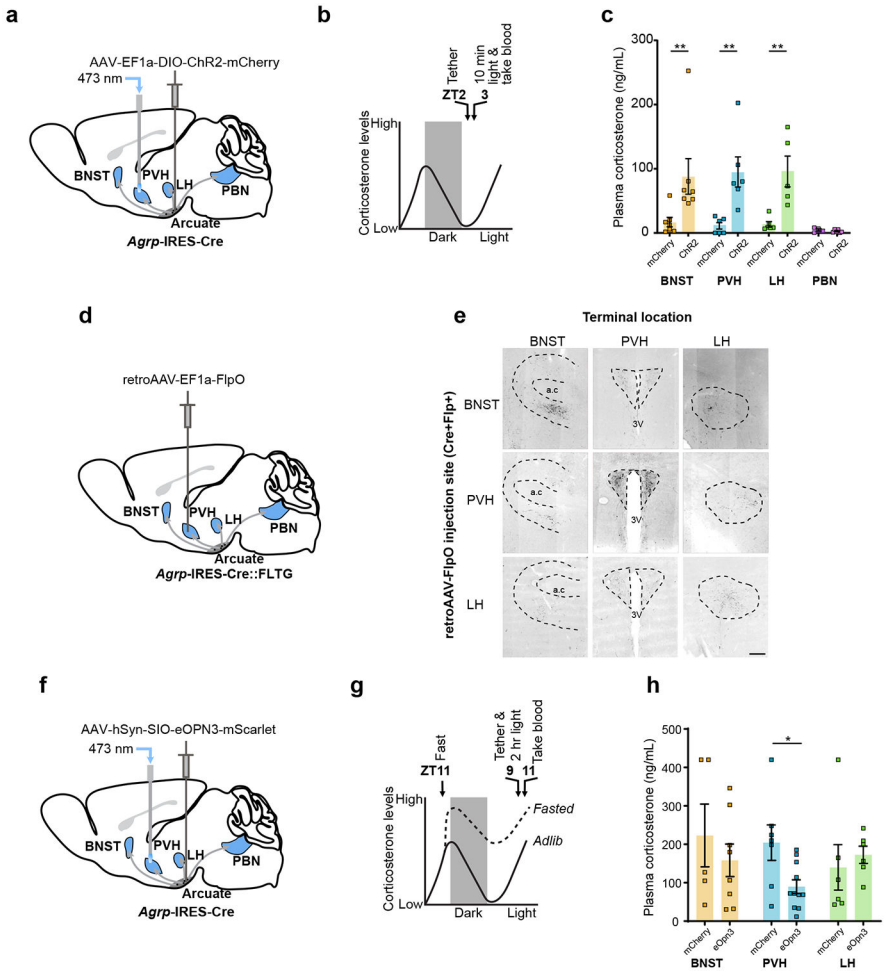

Figure 2. AgRP neurons regulate the HPA axis via projections to the PVH.

a, Schematic of terminal optogenetic stimulation of AgRP neurons. The optic fiber was placed over the PVH (example), BNST, LH or PBN. **b,** Time-line for optogenetic stimulation of AgRP neuron terminals. **c,** Plasma corticosterone levels from mice that received optogenetic stimulation of AgRP neuron terminals in the BNST, PVH, LH or PBN (BNST: $n = 7$ AgRP^{mCherry}, $n = 7$ AgRP$^{ChR2.}$ Mann-Whitney test- $^{**}P = 0.0041$, PVH: $n = 6$ AgRP^{mCherry}, $n = 6$ AgRP^{ChR2}. Mann-Whitney test- $^{**}P = 0.0022$, LH: $n = 6$ AgRP^{mCherry}, $n = 5$ AgRP^{Chr2}. Mann-Whitney test- $^{**}P = 0.0043$, PBN: $n = 4$ AgRP^{mCherry}, $n = 6$ AgRP^{ChR2}. Mann-Whitney test- $P = 0.4762$). **d,** Schematic of collateral mapping via injection of retro-AAV-FlpO into *Agrp*-IRES-Cre::FLTG mice. **e,** AgRP neuron terminals detected upon injection of retro-AAV-FlpO into individual AgRP neuron efferent sites (denoted by row headings) in *Agrp*-IRES-Cre::FLTG mice. a.c: anterior commissure, 3V: third ventricle. **f,** Schematic of terminal inhibition of AgRP neurons. The optic fiber was placed over the PVH (example), BNST or LH. **g,** Time-line for optogenetic inhibition of AgRP neuron terminals and collection of trunk blood. **h,** (BNST: $n = 5$ AgRP^{mCherry}, $n = 8$ AgRP^{eOpn3}. Mann-Whitney test- $P = 0.4973$, PVH: $n = 6$ AgRP^{mCherry}, $n = 11$ AgRP^{eOpn3}. Mann-Whitney test- $^{*}P = 0.0154$, LH: $n = 6$ AgRP^{mCherry}, $n = 6$ AgRP^{eOpn3}. Mann-Whitney test- $P = 0.2403$). Scale bar = 200 μm. Data represent = mean ± sem.

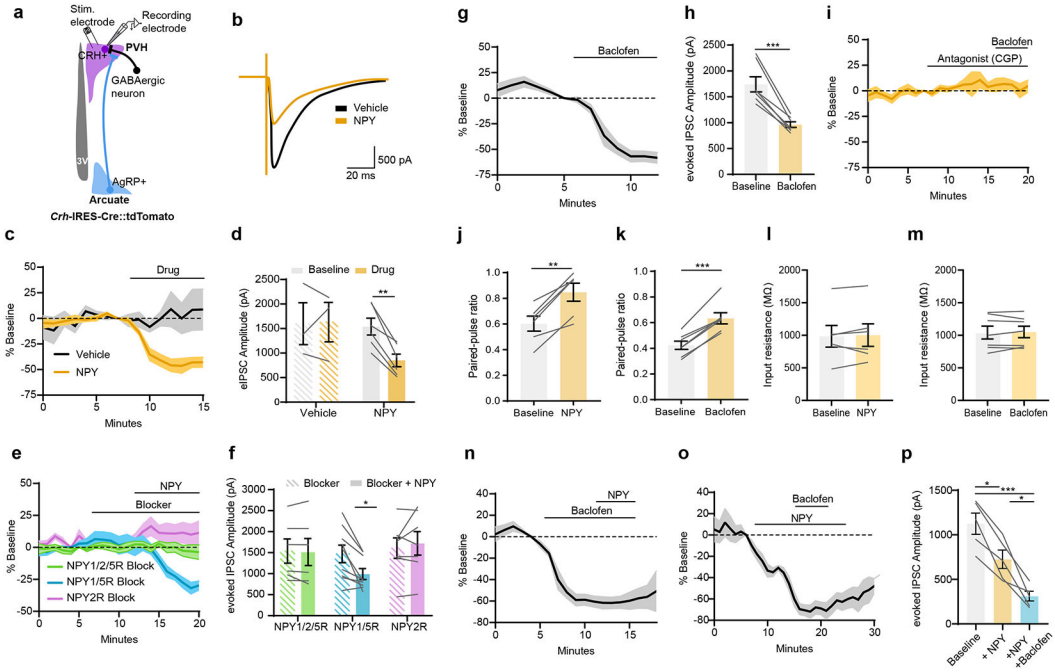

Figure 3. GABA and NPY decrease GABAergic tone onto PVH^{Crh} neurons.

a, Schematic of evoked-IPSC (eIPSCs) recordings from PVH^{Crh} neurons. **b,** Example trace of evoked current amplitude from PVH^{Crh} neurons after Vehicle or NPY treatment. **c,** NPY reduced eIPSC amplitude in PVH^{Crh} neurons (Vehicle: 3 neurons/2 mice; NPY: 6 neurons/3 mice). **d,** Mean eIPSC amplitude in PVH^{Crh} neurons upon drug application (Two-tailed paired *t*-test- $^{**}P = 0.0017$). **e,** NPY2R blocker prevents NPY-mediated reduction in eIPSC amplitude in PVH^{Crh} neurons (NPY1/2/5R blocker: 6 neurons/4 mice; NPY1/5R blocker: 9 neurons/4 mice; NPY2R blocker: 7 neurons/4 mice). **f,** Mean eIPSC amplitude in PVH^{Crh} neurons after NPY + Blockers (NPY1/2/5R Two-tailed unpaired *t*-test- $P = 0.6353$; NPY1/5R Two-tailed unpaired *t*-test- $^{*}P = 0.0216$; NPY2R Two-tailed unpaired *t*-test- $P = 0.6353$). **g,** Baclofen reduced eIPSC amplitude in PVH^{Crh} neurons (7 neurons/6 mice). **h,** Mean eIPSC amplitude in PVH^{Crh} neurons after Baclofen (Two-tailed paired *t*-test- $^{***}P = 0.0004$). **i,** GABA-B-R antagonist prevents baclofen-mediated reduction in eIPSC amplitude in PVH^{Crh} neurons (4 neurons/2 mice). **j, k,** Paired-pulse ratio increased in PVH*Crh* neurons after NPY (**j**) (6 neurons/3 mice. Two-tailed paired *t*-test- $^{**}P = 0.0015$) Baclofen (7 neurons/6 mice. Two-tailed paired *t*-test- $^{***}P = <0.0001$) (**k**). **l, m,** Input resistance was unchanged after NPY (**l**) (6 neurons/3 mice. Two-tailed paired *t*-test- $P = 0.6662$) or Baclofen (**m**) (7 neurons/3 mice. Two-tailed paired *t*-test- $P = 0.7046$). **n,** Time-course of eIPSC amplitude in PVH*Crh* neurons upon application of Baclofen then NPY (7 neurons/6 mice). **o,** Time-course of eIPSC amplitude in PVH*Crh* neurons upon application of NPY then Baclofen (5 cells/3 mice). **p,** Mean eIPSC amplitude in PVH*Crh* neurons after application of NPY, then Baclofen. (One-way ANOVA; Tukey's multiple comparisons. Baseline vs. NPY, $^{*}P = 0.0315$; Baseline vs.+NPY+Baclofen- $^{***}P = 0.0002$; +NPY vs. +NPY+Baclofen- $^{*}P = 0.0256$).

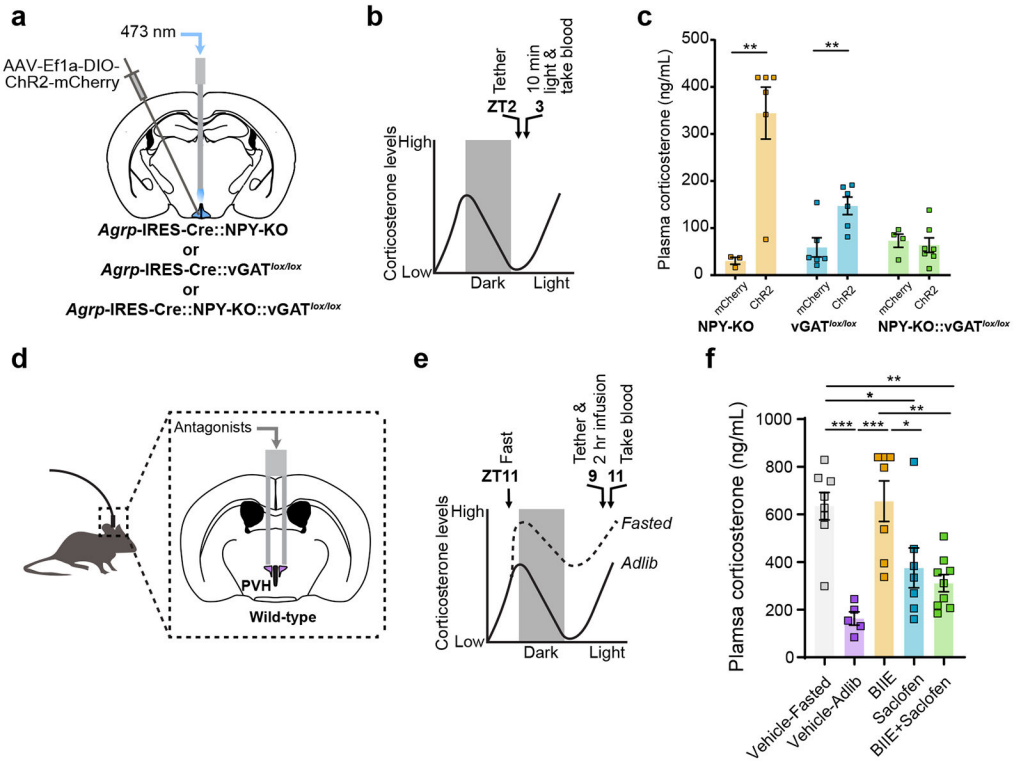

Figure 4. GABA and NPY are required for AgRP neuron regulation of the HPA axis.

a, Schematic of optogenetic stimulation of AgRP neurons in *Agrp*-IRES-Cre::NPY-KO, *Agrp*-IRES-Cre::vGAT$^{lox/lox}$ or *Agrp*-IRES-Cre::NPY-KO::vGAT$^{lox/lox}$ mice. **b**, Time-line for optogenetic stimulation of AgRP neurons. **c,** AgRP-neuron-evoked increase in plasma corticosterone was prevented in *Agrp*-IRES-Cre::NPY-KO::vGAT$^{lox/lox}$ mice (AgRP^{mCherry}::NPY-KO $n = 3$, AgRP^{Chr2}::NPY-KO $n = 6$. Two-tailed unpaired *t*-test- $^{**}P = 0.0060$; AgRP^{mCherry}:: vGAT$^{lox/lox}$ $n = 6$, AgRP^{ChR2}::vGAT$^{lox/lox}$ $n = 6$. Two-tailed unpaired *t*-test- $^{**}P = 0.0095$; AgRP^{mCherry}::NPY-KO::vGAT$^{lox/lox}$ $n = 4$, AgRP^{ChR2}::NPY-KO::vGAT$^{lox/lox}$ $n = 7$. Two-tailed unpaired *t*-test- $P = 0.6946$). **d,** Schematic of *in vivo* drug infusion into the PVH. **e,** Time-line for infusions. **f,** Fasting levels of corticosterone were reduced by intra-PVH GABA-B-R antagonist ± NPY2R antagonist (Vehicle-Fasted $n = 8$, Vehicle-*Ad lib* $n = 5$, BIIE0246 $n = 7$, Saclofen $n = 7$, BIIE0246 + Saclofen $n = 9$. One-way ANOVA, Tukey's multiple comparisons test: Vehicle-Fasted vs. Vehicle-*Ad lib*- $^{***}P = 0.0003$; Vehicle-Fasted vs. BIIE02446- $P = 0.9992$; Vehicle-Fasted vs. Saclofen- $^{*}P = 0.0442$; Vehicle-Fasted vs. BIIE0246+Saclofen- $^{**}P = 0.0039$; Vehicle-*Ad lib* vs. BIIE- $^{***}P = 0.0002$; Vehicle-*Ad lib* vs. Saclofen- $P = 0.2285$; Vehicle-*Ad lib* vs. BIIE0246+Saclofen- $P = 0.5283$; BIIE0246 vs. Saclofen- $^{*}P = 0.0321$; BIIE0246 vs. BIIE0246+Saclofen- $^{**}P = 0.0029$; Saclofen vs. BIIE+Saclofen- $P = 0.9417$). Data represent = mean ± sem.

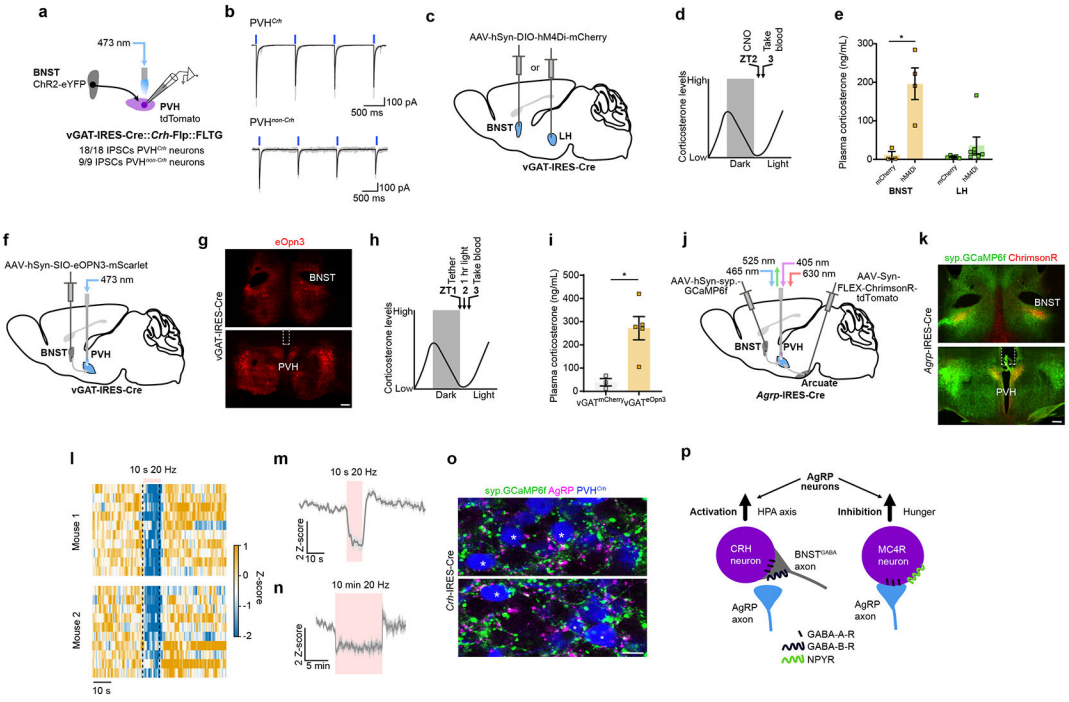

Figure 5. AgRP neurons presynaptically inhibit tonically-active BNST^{GABA} neuron afferents to PVH^{Crh} neurons.

a, Schematic for BNST^{vGAT}→PVH neuron CRACM (n = 18 PVH^{Crh+} neurons, n = 9 PVH^{Crh-} neurons/2 mice). **b,** Representative traces from BNST^{vGAT}→PVH^{Crh+} (upper) and BNST^{vGAT}→PVH^{Crh-} (lower) recordings. **c,** Schematic of BNST or LH injection of Cre-dependent AAV-hM4Di-mCherry into vGAT-IRES-Cre mice. **d,** Time-line of chemogenetic inhibition of BNST^{vGAT} or LH^{vGAT} neurons. **e,** Inhibition of BNST^{vGat} neurons increased corticosterone (BNST: n = 4 vGAT^{mCherry}, n = 4 vGAT^{hM4Di}. Two-tailed unpaired t-test- *P = 0.0131; LH: n = 5 vGAT^{mCherry}, n = 7 vGAT^{hM4Di}. Two-tailed unpaired t-test- P = 0.2837). **f,** Schematic of BNST^{vGAT}→PVH terminal inhibition. **g,** Representative eOpn3 expression in the BNST (upper) and location of optic fibers in the PVH (lower). **h,** Time-line for terminal inhibition of BNST^{vGAT}→PVH projections. **i,** Inhibition of BNST^{vGAT}→PVH projections increased corticosterone (n = 3 vGAT^{mCherry}, n = 5 vGAT^{eOpn3}. Two-tailed unpaired t-test- *P = 0.0076). **j,** Schematic of BNST→PVH terminal recordings with optogenetic stimulation of AgRP→PVH terminals. **k,** Representative images of synaptophysin-GCaMP6f expression in BNST neurons and terminals and ChrimsonR-tdTomato expression in AgRP neuron terminals. **l,** Heatmaps of BNST→PVH fiber photometry recordings from two mice. **m, n,** Optogenetic stimulation of AgRP→PVH terminals for 10 sec at 20 Hz (**m**) (n = 3 mice) and 10 min at 20 Hz (**n**) (n = 4 mice) reduced activity of BNST→PVH terminals. **o,** Representative images of BFP-labelled PVH^{Crh} neurons, synaptophysin-GCaMP6f-expressing BNST neuron terminals and AgRP immunofluorescence (* = PVH^{Crh} neurons apposed by BNST and AgRP neuron terminals). **p,** Schematic of AgRP neuron action in the PVH. Left = presynaptic disinhibition of PVH^{Crh} neurons by GABA/presynaptic GABA-B-Rs. Right = monosynaptic inhibition of PVH^{Mc4r}

neurons by GABA/postsynaptic GABA-A-Rs. Scale bar (**g**, **k**) = 200 μm. Scale bar (**o**) = 10 μm. Data represent = mean ± sem.